


TITLE: Afferent and efferent projections of the anterior cortical amygdaloid nucleus in the mouse.

AUTHORS: Bernardita Cádiz-Moretti¹, María Abellán-Álvaro¹, Cecília Pardo-Bellver¹, Fernando Martínez-García² and Enrique Lanuza^{1*} 

¹ Unitat Mixta de Neuroanatomia Funcional UV-UJI – Dept. de Biologia Cel·lular i Biologia Funcional, Facultat de Ciències Biològiques, Universitat de València. Burjassot 46100, València, Spain.

² Unitat Mixta de Neuroanatomia Funcional UV-UJI - Unitat Predepartamental de Medicina, Fac. Ciències de la Salut, Universitat Jaume I. Castelló de la Plana, Spain.

NUMBER OF TEXT PAGES: 45

NUMBER OF FIGURES: 8

NUMBER OF TABLES: 2

ABBREVIATED TITLE: Anterior cortical amygdala connections

KEY WORDS: vomeronasal; olfactory system; chemosensory amygdala; fluorogold; axonal tracing; RRID: AB_90738

*Correspondence to: Enrique Lanuza. Dept. de Biologia Cel·lular. Facultat de Ciències Biològiques. Universitat de València. C/ Dr. Moliner, 50. ES-46100, Burjassot. València. Spain. E-mail: Enrique.Lanuza@uv.es

Phone: 34 96 354 33 83 Fax: 34 96 354 34 04.

FUNDING

This article has been accepted for publication and undergone full peer review but has not been through the copyediting, typesetting, pagination and proofreading process which may lead to differences between this version and the Version of Record. Please cite this article as an 'Accepted Article', doi: 10.1002/cne.24248

© 2017 Wiley Periodicals, Inc.

Received: Jan 11, 2017; Revised: May 11, 2017; Accepted: May 11, 2017

Funded by the Spanish Ministry of Economy and Competitiveness-FEDER (BFU2013-47688-P; BFU2016-77691-C2-2-P and C2-1-P) and the Generalitat Valenciana (PROMETEO/2016/076). B.C.-M. is a predoctoral fellow of the “Becas Chile” program of the Government of Chile. C.P.-B. is a predoctoral fellow of the “Atracció de Talent” program of the University of València. M.A.-A is a fellow of the “Programa de Empleo Joven” PEJ-2014-A-63220 of the Spanish Government.

Accepted Article

ABSTRACT (max. 250 words)

The anterior cortical amygdaloid nucleus (ACo) is a chemosensory area of the cortical amygdala that receives afferent projections from both the main and accessory olfactory bulbs. The role of this structure is unknown, partially due to a lack of knowledge of its connectivity. In this work, we describe the pattern of afferent and efferent projections of the ACo by using fluorogold and biotinylated dextranamines as retrograde and anterograde tracers, respectively. The results show that the ACo is reciprocally connected with the olfactory system and basal forebrain, as well as with the chemosensory and basomedial amygdala. In addition, it receives dense projections from the midline and posterior intralaminar thalamus, and moderate projections from the posterior bed nucleus of the stria terminalis, mesocortical structures and the hippocampal formation. Remarkably, the ACo projects moderately to the central nuclei of the amygdala and anterior bed nucleus of the stria terminalis, and densely to the lateral hypothalamus. Finally, minor connections are present with some midbrain and brainstem structures.

The afferent projections of the ACo indicate that this nucleus might play a role in emotional learning involving chemosensory stimuli, such as olfactory fear conditioning. The efferent projections confirm this view and, given its direct output to the medial part of the central amygdala and the hypothalamic ‘aggression area’, suggest that the ACo can initiate defensive and aggressive responses elicited by olfactory or, to a lesser extent, vomeronasal stimuli.

ABBREVIATIONS

I	layer 1
II	layer 2
2Cb	2nd Cerebellar lobule
III	layer 3
3V	3rd ventricle
4V	4th ventricle
AAD	anterior amygdaloid area, dorsal part
AAV	anterior amygdaloid area, ventral part
AC	anterior commissural nucleus
aca	anterior commissure, anterior part
ACb	nucleus accumbens
AcbC	accumbens nucleus, core
AcbSh	accumbens nucleus, shell
ACo	anterior cortical amygdaloid nucleus
acp	anterior commissure, posterior part
ADP	anterodorsal preoptic nucleus
AH	anterior hypothalamic area
AHA	anterior hypothalamic area, anterior part
AHi	amygdalohippocampal area
AHP	anterior hypothalamic area, posterior part
AI	agranular insular cortex
AID	agranular insular cortex, dorsal part
AIP	agranular insular cortex, posterior part
AIV	agranular insular cortex, ventral part
AOB	accessory olfactory bulb
AOL	anterior olfactory nucleus, lateral part
AOM	anterior olfactory nucleus, medial part
AON	anterior olfactory nucleus
AOP	anterior olfactory nucleus, posterior part
APir	amygdalopiriform transition area
Aq	aqueduct
Arc	arcuate nucleus
Astr	amygdalostriatal transition area
BAOT	bed nucleus of the accessory olfactory
BLA	basolateral amygdaloid nucleus, anterior part
BLP	basolateral amygdaloid nucleus, posterior part
BLV	basolateral amygdaloid nucleus, ventral part
BMA	basomedial amygdaloid nucleus, anterior part
BMP	basomedial amygdaloid nucleus, posterior part
BST	bed nucleus of the <i>stria terminalis</i>
BSTIA	BST, intraamygdaloid division
BSTLD	BST, lateral division, dorsal part
BSTLP	BST, lateral division, posterior part
BSTLV	BST, lateral division, ventral part
BSTMA	BST, medial division, anterior part
BSTMPI	BST, medial division, posterointermediate part
BSTMPL	BST, medial division, posterolateral part
BSTMPM	BST, medial division, posteromedial part
BSTMV	BST, medial division, ventral part

CA1	field CA1 of hippocampus
CA3	field CA3 of hippocampus
Ce	central amygdaloid nucleus
CeC	central amygdaloid nucleus, capsular part
CeL	central amygdaloid nucleus, lateral division
CeM	central amygdaloid nucleus, medial division
Cl	claustrum
CM	central medial thalamic nucleus
cp	cerebral peduncle
CPu	caudate putamen
CxA	cortex-amygdala transition zone
D3V	dorsal 3rd ventricle
DEn	dorsal endopiriform nucleus
DG	dentate gyrus
dlo	dorsal lateral olfactory tract
DM	dorsomedial hypothalamic nucleus
DP	dorsal peduncular cortex
DPMe	deep mesencephalic nucleus
DR	dorsal raphe nucleus
DTT	dorsal <i>tenia tecta</i>
E/OV	ependymal and subependymal layer/olfactory ventricle
ec	external capsule
eml	external medullary lamina
Ect	ectorhinal cortex
EPI	external plexiform layer of the main olfactory bulb
EPIA	external plexiform layer of the accessory olfactory bulb
f	fornix
fr	<i>fasciculus retroflexus</i>
Gl	glomerular layer of the main olfactory bulb
GIA	glomerular layer of the AOB
GrA	granule cell layer of the AOB
GrO	granular cell layer of the main olfactory bulb
HDB	nucleus of the horizontal limb of the diagonal band
I	intercalated nuclei of the amygdala
ic	internal capsule
IF	interfascicular nucleus
IL	infralimbic cortex
IM	intercalated amygdaloid nucleus, main part
IMD	intermediodorsal thalamic nucleus
IP	interpeduncular nucleus
IPAC	interstitial nucleus of the posterior limb of the anterior commissure
IPI	internal plexiform layer of the main olfactory bulb
LA	lateroanterior hypothalamic nucleus
La	lateral amygdaloid nucleus
LaDL	lateral amygdaloid nucleus, dorsolateral part
LaVL	lateral amygdaloid nucleus, ventrolateral part
LaVM	lateral amygdaloid nucleus, ventromedial part
LC	<i>locus coeruleus</i>
LDTg	laterodorsal tegmental nucleus
LEnt	lateral entorhinal cortex

LGP	lateral <i>globus pallidus</i>
LH	lateral hypothalamic area
LHb	lateral habenula
LMol	<i>lacunosum molculare</i> layer
LPAG	lateral periaqueductal gray
LPB	lateral parabrachial nucleus
LPO	lateral preoptic area
LO	lateral orbital cortex
lo	lateral olfactory tract
LOT	nucleus of the lateral olfactory tract
LSD	lateral septal nucleus, dorsal part
LSI	lateral septal nucleus, intermediate part
LSV	lateral septal nucleus, ventral part
LV	lateral ventricle
MCLH	magnocellular nucleus of the lateral hypothalamus
MCPO	magnocellular preoptic nucleus
MD	mediodorsal thalamic nucleus
Me	medial amygdaloid nucleus
MeA	medial amygdaloid nucleus, anterior subnucleus
me5	mesencephalic trigeminal tract
MeAD	medial amygdaloid nucleus, anterodorsal part
MeAV	medial amygdaloid nucleus, anteroventral part
MePD	medial amygdaloid nucleus, posterodorsal subnucleus
MePV	medial amygdaloid nucleus, posteroventral subnucleus
MGD	medial geniculate nucleus, dorsal part
MGM	medial geniculate nucleus, medial part
MGV	medial geniculate nucleus, ventral part
Mi	mitral cell layer of the main olfactory bulb
MiA	mitral cell layer of the AOB
ml	medial lemniscus
mlf	medial longitudinal fasciculus
MnPO	median preoptic nucleus
MO	medial orbital cortex
MOB	main olfactory bulb
MPA	medial preoptic area
MPB	medial parabrachial nucleus
MPO	medial preoptic nucleus
MS	medial septal nucleus
mt	mamillothalamic tract
mtg	mamillotegmental tract
Mtu	medial tuberal nucleus
ns	nigrostriatal bundle
opt	optic tract
Pa	paraventricular hypothalamic nucleus
PAG	periaqueductal gray
PB	parabrachial nucleus
pc	posterior commissure
Pe	periventricular hypothalamic nucleus
PF	parafascicular thalamic nucleus
PH	posterior hypothalamic area

PIL	posterior intralaminar thalamic nucleus
Pir	piriform cortex
PLCo	posterolateral cortical amygdaloid nucleus
PMCo	posteromedial cortical amygdaloid nucleus
PMD	premamillary nucleus, dorsal part
PMV	premamillary nucleus, ventral part
PMnR	paramedian part of the raphe nucleus
PN	paranigral nucleus
PnC	pontine reticular nucleus, caudal part
PnO	pontine reticular nucleus, oral part
PoT	triangular part of the posterior thalamic nucleus
PP	peripeduncular nucleus
PPTg	pedunculopontine tegmental nucleus
PRh	perirhinal cortex
PrL	prelimbic cortex
PS	parastrial nucleus
PSTh	parasubthalamic nucleus
PT	paratenial thalamic nucleus
pv	periventricular fiber system
PV	paraventricular thalamic nucleus
PVA	paraventricular thalamic nucleus, anterior part
PVP	paraventricular thalamic nucleus, posterior part
Py	pyramidal cell layer of the hippocampus
py	pyramidal tract
Rad	<i>stratum radiatum</i> of hippocampus
RCh	retrochiasmatic area
Re	reuniens thalamic nucleus
Rh	rhomboid thalamic nucleus
RLi	rostral linear nucleus of the raphe
RMC	red nucleus, magnocellular part
RPC	red nucleus, parvicellular part
S	subiculum
SCh	suprachiasmatic nucleus
scp	superior cerebellar peduncle
SG	suprageniculate thalamic nucleus
SHi	septohippocampal nucleus
SHy	septohypothalamic nucleus
SI	<i>substantia innominata</i>
SL	semilunar nucleus
sm	<i>stria medullaris</i>
SM	nucleus of the <i>stria medullaris</i>
SNC	<i>substantia nigra</i> , compact part
SNR	<i>substantia nigra</i> , reticular part
sp5	spinal trigeminal tract
SPF	subparafascicular thalamic nucleus
SPFPC	subparafascicular thalamic nucleus, parvicellular part
st	<i>stria terminalis</i>
SuM	supramamillary nucleus
Subl	subincertal nucleus
STh	subthalamic nucleus

TC	<i>tuber cinereum</i> area
Te	terete hypothalamic nucleus
Tu	olfactory tubercle
unc	<i>uncinate fasciculus</i>
VDB	nucleus of the vertical limb of the diagonal band
VE _n	ventral endopiriform nucleus
VMH	ventromedial hypothalamic nucleus
VP	ventral pallidum
VTA	ventral tegmental area
VTM	ventral tuberomammillary nucleus
VTT	ventral tenia tecta
ZI	<i>zona incerta</i>

INTRODUCTION

The discovery of the critical role of the basolateral and central amygdaloid nuclei in fear learning has led to an extensive research focused on these areas (Janak and Tye, 2015), while the chemosensory structures of the amygdala have received much less attention. However, the chemosensory areas of the amygdaloid complex are important for controlling social, sexual and maternal behaviors in rodents (Swann et al., 2009). These areas may also play a relevant role in emotional learning, as shown in the case of olfactory fear conditioning, in which a previously neutral odor becomes aversive by its association to a footshock (Cousen and Otto, 1998; Sevelinges et al., 2004). Among the amygdaloid structures involved in chemosensory-mediated emotional behavior, the medial amygdaloid nucleus (Me) has been by far the most studied, since lesions of this nucleus abolish the chemosensory control of sexual behaviors (Lehman et al., 1980). However, the Me is (mainly) a subcortical structure (Swanson and Petrovich, 1998) with a heterogeneous embryological origin (Bupesh et al., 2011). Therefore, the Me is probably an output station, controlled by its cortical inputs. One of its relevant cortical inputs originates in its neighbor structure, the anterior cortical nucleus of the amygdala (ACo) (Cádiz-Moretti et al., 2016a). Recent electrophysiological studies have revealed that the ACo provides an olfactory input to the Me which synapses into vomeronasally-driven Me neurons, allowing the integration of olfactory and vomeronasal information at the single cell level (Keshavarzi et al., 2015; see Guthman and Vera, 2016). In addition, the ACo (as the Me), receives direct projections arising from the main and accessory olfactory bulbs (Scalia and Winans, 1975; Pro-Sistiaga et al., 2007; Kang et al., 2009; Cádiz-Moretti et al., 2013). These convergent projections may allow olfactory and vomeronasal information to be integrated in this structure. The ACo has also been suggested, based on electrophysiological data, to play a role in olfactory fear conditioning (Sevelinges et al., 2004). Therefore, this cortical amygdaloid structure seems to be an associative nucleus involved in olfactory learning processes (either olfactory-vomeronasal associations or olfactory fear learning). However, the connectivity of ACo that may underlie these associative processes, and in turn influence behavioral responses, is unknown.

To our knowledge, a comprehensive study of the connectivity of the ACo has not been performed in mice. Partial information on its afferent connections is derived mainly from early studies based on injections of retrograde tracers in the amygdala of rats

(Veening, 1978a, 1978b; Ottersen and Ben-Ari, 1979; Ottersen, 1980; Ottersen, 1982), as well as descriptions of the efferent projections of some structures that project to the ACo (mainly in rats, see McDonald, 1998, for cortical projections, and Pitkänen, 2000, for intraamygdaloid connections). With regard to the efferent projections, data are available for rats (Luskin and Price, 1983; Petrovich et al., 1996), cats (Krettek and Price, 1977) and hamsters (Kevetter and Winans, 1981). In contrast to the lack of anatomical studies in mice, functional data in female mice have shown that the ACo exhibits Fos immunoreactive cells induced by exposure to male urinary odors (Moncho-Bogani et al., 2005; Martel and Baum, 2009; Brock et al., 2012). Moreover, Majkutewicz et al. (2010) showed in rats that the ACo, in addition with other mesolimbic structures, displayed increased Fos expression after electrical stimulation of the ventral tegmental area. These authors suggested that the ACo might play a role in ingestive and exploratory behaviors due to its role in processing the reinforcing properties of olfactory stimuli.

This work is part of a long-term project aiming to provide a complete description of the connectivity of the chemosensory amygdala in mice. We have previously reported the connections of the Me (Pardo-Bellver et al., 2012; Cádiz-Moretti et al., 2016a), the posteromedial cortical nucleus of the amygdala (Gutiérrez-Castellanos et al., 2014) and the cortex-amygdala transition zone (Cádiz-Moretti et al., 2016b), as well as the connection of the chemosensory amygdaloid structures with the ventral striatum (Úbeda-Bañón et al., 2007; 2008; Novejarque et al., 2011). The aim of this work is to provide a comprehensive description of the afferent and efferent connections of the ACo in mice, which is currently lacking. With this description, we want to highlight the possible importance of this structure in the processing of convergent vomeronasal and olfactory information, as well as to clarify other inputs and outputs relevant to the processing of chemosensory information in this cortical amygdaloid area.

MATERIAL AND METHODS

Animals

For the present study, we used 15 adult female mice (*Mus musculus*) from the CD1 strain (Janvier, Le Genest Saint-Isle, France), which were 9-27 weeks old and weighed 27.8-51.1 g at the beginning of the experiments. They were kept in cages with food and water *ad libitum* in a 12 h light:dark cycle at 22-24 °C. We treated the mice according to

the guidelines of the European Union Council Directive of June 3rd, 2010 (6106/1/10 REV1). The Committee of Ethics on Animal Experimentation of the University of Valencia approved all the experimental procedures.

Surgery and tracer injections

For surgery, animals were anesthetized with isoflurane (2-2.5%) in oxygen (1-1.3 L/min) (MSS Isoflurane Vaporizer, Medical Supplies and Services, UK) delivered through a mouse anesthetic mask attached to the stereotaxic apparatus (David Kopf, 963-A, Tujunga CA, USA). Analgesia was provided by subcutaneous butorphanol (5 mg/kg, Turbugesic, Pfizer, New York, USA). While the head was fixed in the stereotaxic, mice rested on a thermal blanket to keep their body temperature, and eye drops (Siccafluid, Thea S.A. Laboratories, Spain) were used to prevent eye ulceration.

Tract-tracing experiments were performed by means of iontophoretic injections of the fluorescent retrograde tracer Fluoro-Gold (FG, hydroxystilbamidine bis (methanesulfonate), Sigma-Aldrich, Cat # 39286) diluted at 2% in distilled water, and the anterograde tracer biotin-conjugated dextranamine (BDA, 10,000 MW, lysine fixable, Invitrogen, Carlsbad, CA, USA), diluted at 5% in phosphate buffer (PB) 0.01M, pH 8.0. To reduce the number of animals, FG was injected in one hemisphere and BDA in the other. Tracer injections were performed with glass micropipettes (20-30 μm diameter tips) by means of positive current pulses (7on/7off) of 2-3 μA over the course of 3-6 minutes, and the micropipette was left in place for 10 minutes after finishing the injection. To avoid diffusion of the tracer along the pipette track, a continuous retention current (-0.1 μA) was applied during the entrance and withdrawal of the micropipette. Stereotaxic coordinates relative to Bregma were taken from the atlas of the mouse brain (Paxinos and Franklin, 2004), and applied, using a flat skull approach, as follows: AP - 0.8 to - 1.5 mm, L - 2.55 to -2.8 mm and DV -5.97 to -6.02 mm. After the injection, we closed the wound with Histoacryl (Braun, Tuttlinger, Germany).

Histology

After 7-8 days of survival, we deeply anaesthetized the animals with an intraperitoneal injection of sodium pentobarbital (100mg/kg, Eutanax, Laboratorios Normon S.A. Madrid, Spain) and perfused them transcardially with saline solution (0.9%) followed by 4% paraformaldehyde (diluted in PB 0.1M, pH 7.6). Following perfusions, brains

were removed from the skulls, postfixed for 4 hours in the same fixative and cryoprotected in 30% sucrose in PB (0.1M, pH 7.6) at 4°C until they sank. We used a freezing microtome to obtain sagittal sections (30 µm) through the olfactory bulbs and frontal sections (40 µm) through the rest of the brain. In both cases, sections were collected in four parallel series.

After checking the location and extent of the FG injection deposits using fluorescence microscopy, we processed one of the series of each brain for the simultaneous detection of BDA and FG in free-floating sections. For the histochemical detection of the BDA, endogenous peroxidase was inactivated with 1% H₂O₂ in Tris-buffered saline (TBS; 0.05 M, pH 7.6) for 15 min at room temperature and then sections were incubated for 90 min in ABC complex (Vectastain ABC kit, Vector Labs, PK-6100, Burlingame, CA, USA) diluted 1:50 in TBS-Tx (0.3% Triton X-100 in 0.05 M TBS, pH 7.6). After rinsing the sections thoroughly with TBS, peroxidase activity was visualized with 0.025% diaminobenzidine in TB (0.1 M, pH 8.0) as chromogen, 0.01% H₂O₂ as substrate, and 0.1% nickel ammonium sulfate as enhancer, yielding a black precipitate as reaction product. Subsequently, FG was immunohistochemically detected in the same sections. To do so, sections were incubated in a blocking solution of TBS-Tx containing 8% normal goat serum (NGS) and 4% bovine serum albumin (BSA) for 2 hours at room temperature. Then, sections were sequentially incubated in (Table 1): rabbit anti-FG (Millipore, Cat # AB153, RRID: AB_90738) diluted 1:3000 in TBS-Tx with 4% NGS and 2% BSA overnight at 4°C; biotinylated goat anti-rabbit IgG (Vector, Cat # BA-1000) diluted 1:200 in TBS-Tx with 4% NGS for 2 hours at room temperature; and ABC Elite diluted 1:50 in TBS-Tx for 2 hours at room temperature. Finally, the resulting peroxidase labeling was revealed with 0.025% diaminobenzidine in TB (0.1M, pH 8.0) with 0.01% H₂O₂. The resulting precipitate was a brown product, easily distinguishable from the black precipitate resulting from the histochemical detection of BDA. For some of the animals, an additional series was processed only for the detection of BDA and counterstained with Nissl.

The specificity of the anti-FG antibody has been previously characterized, and this antibody has been extensively used in our laboratory (e.g. Gutiérrez- Castellanos et al., 2014; Cádiz-Moretti et al., 2016a, 2016b). The omission of the primary antibody or

performing the immunohistochemical procedure in animals with no FG injection yielded no labeling.

In addition, to determine the boundaries, extent and cytoarchitectonic organization of the ACo, we brain sections stained with Nissl and acetyl cholinesterase (AChE) histochemistry available at the laboratory. AChE histochemistry was performed according to Geneser-Jensen and Blackstad (1971). Briefly, sections were incubated in a medium containing 4mM acetylthiocholine, 2mM CuSO₄, 10mM glycine and 0.2mM ethopropazide in 50mM acetate buffer (pH 5.5) for 2-3 h at 37°C. After rinsing, AChE activity was visualized during 1 min of incubation in 10% potassium ferricyanide.

Sections were mounted onto gelatinized slides, dehydrated in alcohols, cleared with xylene and cover-slipped with Entellan (Merck Millipore).

Image acquisition and processing

We observed the sections using an Olympus CX41RF-5 microscope and photographed them using a digital Olympus XC50 camera. Fluorescent images of the FG injection sites were observed with a Leitz DMRB microscope with epifluorescence (Leica EL-6000) equipped with a specific filter for FG (Leica, A) and imaged using a digital Leica DFC 300 FX camera. Using Adobe Photoshop 7.0 (Adobe Systems, MountainView, CA, USA) pictures were flattened by subtracting background illumination and brightness and contrast were optimized. No further changes were performed. Finally, illustrations were designed with Adobe Photoshop 7.0 and Illustrator.

The distribution of labeled structures after the tracer injections was mapped using one of the restricted FG and BDA injections as a model. To do so, selected microscopic images were imported into Adobe Illustrator CS6 (Adobe Systems) and the limits of the brain areas were drawn using as a reference the atlas by Paxinos and Franklin (2004). Anterograde and retrograde labeling were charted representing, in a roughly proportional manner, the density of fibers and terminals or neuronal somata, respectively. The labeling density was considered as very dense, dense, moderate, scarce, and very scarce (see Table 2). As a reference (see Fig. 1), we considered very dense the retrograde labeling in the mitral cell layer of the main olfactory bulb, and very scarce the presence of only 2–5 labeled cell bodies. In the case of anterograde labeling, we considered very dense the labeling observed in the posterolateral cortical

amygdaloid nucleus, and very scarce the presence of only 2–5 labeled fibers. The density of labeling was rated in each of the restricted injections (three of FG and four of BDA) by one researcher, and confirmed independently by two other researchers, specially focusing in the structures in which the different experimental cases have yielded more variability.

RESULTS

We first describe the architecture and chemoarchitecture of the ACo, which are helpful to delineate the location and extent of the tracer injections. Then we report the distribution and relative density of retrogradely labeled cells observed after FG injections, and the pattern of anterograde labeling resulting after the BDA experiments. For the description of the retrograde and anterograde labeling, we follow the cytoarchitecture and nomenclature of the atlas of Paxinos and Franklin (2004).

Cytoarchitecture and chemoarchitecture of the ACo

The ACo is characteristically negative for AchE activity, with clear boundaries with the laterally adjacent cortex-amygdala transition area (CxA), which is moderately reactive, and the medially adjacent nucleus of the lateral olfactory tract (LOT), which is strongly reactive (Fig. 2A', B', C'). At caudal levels, however, it shows no clear boundary with the anterior division of the Me (Fig. 2D'). From the cytoarchitectural point of view, it shows a trilaminar organization, albeit less obvious than that of the adjacent CxA (Fig. 2A-D). ACo shows a relatively loose organization of the cell layer, in which the boundary between layers II and III is difficult to discern (Fig. 2A-D). This laminar organization is more obvious at caudal levels, and can hardly be observed at the rostral tip of the structure (compare Fig. 2A with Fig. 2D). The deep border of layer III is also quite diffuse, at both rostral and caudal levels, where the ACo limits with the dorsal anterior amygdaloid area and anterior basomedial nucleus (BMA) respectively. The neuropil of the BMA shows positive immunoreactivity for calretinin, while the deep layer of the ACo is only moderately reactive (Martínez-García et al., 2012). However, the boundary between the two structures is diffuse (Fig. 2D-D').

Retrograde labeling after FG injections into the anterior cortical amygdaloid nucleus

Eight injections targeted the ACo, three of which displayed FG deposits that were restricted to this nucleus (Fig. 3A-D). The location of the injection sites was determined by means of fluorescence microscopy, since the labeled cells were more evident against the background fluorescence than in the immunolabeled sections. The extent of the effective injection site was considered as the area showing aggregated FG-labeled cells clearly stained above background (see Fig 3J). Two of the restricted injections involved the superficial layer I (cases #1339 and #1245) and one was mainly located in layer II (case #1321). For two of the three injection cases, traces of FG could be observed along the micropipette track in the caudoputamen, the lateral globus pallidus and the central amygdaloid nucleus (cases #1321 and #1339). Additionally, three more injections were centered in ACo, but extended to CxA, and in other two cases the injections affected the ACo and the posterolateral cortical amygdaloid nucleus (PLCo), which is caudolaterally adjacent. The pattern of labeling was similar in all the restricted injections (case #1339 is illustrated in Fig. 4). In the non-restricted injections, the resulting labeling included the pattern observed in the restricted ones, as well as labeling due to the CxA (Cádiz-Moretti et al., 2016b) or the PLCo (Úbeda-Bañón et al., 2007).

In general, the ACo injections gave rise to a high density of retrograde labeling in the olfactory system, the chemosensory amygdala and the posterior intralaminar thalamus. In addition, the central and basolateral complex of the amygdala, several subnuclei of the bed nucleus of the *stria terminalis* (BST) complex, some cortical areas, the hippocampal formation, the septum and striatum, and several hypothalamic, mesencephalic and brainstem nuclei presented retrograde labeling in a degree from moderate to very scarce (Table 2).

Retrograde labeling in the olfactory system

After the injections of FG in the ACo, very dense labeling was observed throughout the mitral cell layer of the main olfactory bulb (MOB; Table 2, Figs. 1A, 4A and 5A). The somata of the mitral cells was darkly stained. Moreover, a few labeled cells were present in the external plexiform layer of the MOB (which may be tufted cells), as well as in the internal plexiform layer and in the glomerular layer of the MOB. The accessory olfactory bulb (AOB) also showed retrograde labeling in the mitral cell layer and a few labeled cells in its glomerular layer (Table 2, Figs. 1B, 4A and 5A), especially in the cases with superficial injections (cases #1245 and #1339).

Regarding the olfactory structures, some areas such as the piriform cortex (Pir) and endopiriform nucleus showed remarkable retrograde labeling. The Pir displayed a heterogeneous pattern of labeling along its rostro-caudal extent (Fig. 4B-F). In the anterior Pir, a moderate number of labeled cells was present in the inner layer II (Table 2; Fig. 4B). In addition, layer I displayed a few labeled cells located just below the lateral olfactory tract. At intermediate levels of the Pir, labeling was dense and the labeled cells were distributed homogeneously through layers II and III (Fig. 4C-E and 5C). Finally, in the caudal Pir, the density of labeling was moderate (Fig. 4F and 5D). Remarkably, in the most rostral injection (case #1339), the density of labeling along the Pir was higher than in the other two injections. The dorsal endopiriform nucleus also presented a heterogeneous labeling, showing more labeled somata in its rostral than its caudal part, while the ventral endopiriform nucleus showed a moderate number of labeled cells all along its rostrocaudal extent (Table 2, Fig. 4B-F and Fig. 5C, D). Both the Pir and the ventral endopiriform nucleus displayed darkly stained somata. The dorsal *tenia tecta* also showed a moderate number of labeled somata, mainly located in its layer III (Table 2) whereas in the ventral *tenia tecta* only scarce labeled cells were observed, most of which located in layer II (Table 2, not shown). Finally, a low density of labeled cell bodies was also observed in the three divisions (lateral, posterior, and medial) of the anterior olfactory nucleus (Table 2, Fig. 5B) and at the territory located just medial to the posterior aspect of the anterior olfactory nucleus (Fig. 5B).

Retrograde labeling in the amygdala

Within the amygdaloid complex, the nuclei composing the chemosensory amygdala displayed the densest populations of retrograde labeled cells. In addition, FG injections in the ACo rendered noticeable retrograde labeling in some deep nuclei of the amygdala, namely the central and basolateral divisions as well as the amygdalohippocampal area.

In the olfactory amygdala (Table 2), ACo injections gave rise to a dense population of retrogradely labeled cells in the CxA (in its layers II and III) and in the LOT (mainly in layer II) (Fig. 4C-D). More caudally, labeled somata in the three layers of the PLCo, with more labeled cells observed in the rostral than in the caudal aspect of this nucleus (Fig. 4D-F and Fig. 5C, D). Adjacent to the caudal PLCo, the amygdalopiriform

transition area displayed a moderate number of labeled cells (Table 2, Fig. 4F, G and Fig. 5D).

In the vomeronasal amygdala (Table 2), injections located in the superficial ACo gave rise to very dense labeling in the bed nucleus of the accessory olfactory (BAOT), while in the deep injection labeling was moderate-to-dense (not shown). In addition, a moderate number of labeled cells was observed in the ventral and dorsal parts of the anterior amygdaloid area, as well as in the three subdivisions of the Me (Table 2, Fig. 4C-E and Fig. 5C), where labeled neurons concentrate in the cell layer. Within the posterodorsal subnucleus of the Me, labeled cell bodies appeared mainly aligned in the outer limit of its cell layer (Figs. 4E and 5C). Caudally, a heterogeneous labeling was present in the posteromedial cortical amygdaloid nucleus (PMCo), with the labeled somata located in its cellular layer (Fig 4E-G). Its rostral part was almost depleted of retrograde labeling (Fig. 4E and 5C), while its caudal part showed a dense number of labeled somata (Fig. 4F, G and 5D).

In the basolateral amygdaloid division, the anterior (BMA) and posterior part (BMP) of the basomedial amygdaloid nucleus showed a moderate density of labeled cells (Table 2, Fig. 4C-F and Fig. 5C, D), with the BMA showing an especially dense population of labeled neurons in its rostral portion, next to the injection site (compare Fig. 4C and 4D). Concerning the basolateral nucleus, labeling was scarce in its posterior and ventral subnuclei and very scarce in the anterior division (Table 2, Fig. 4D-F and Fig. 5C, D). Within the lateral nucleus, only the dorsolateral division showed consistent labeling, but always with a low number of labeled neurons (Table 2; Fig. 4D, E). In addition, the ventrolateral part of the lateral amygdaloid nucleus displays a few scattered cells in one injection. The amygdalohippocampal area presented also scarce labeling (Table 2, Fig. 4E, F and Fig. 5D). Finally, regarding the central amygdala, it showed a few labeled cells, mainly in its medial subdivision (Table 2, Fig. 4D, E).

Retrograde labeling in the bed nucleus of the stria terminalis (BST)

In general, retrograde labeling in the BST was moderate or scarce. The posterointermediate part of medial division of BST (BSTMPI, Fig. 4C) and the intraamygdaloid division of the BST (BSTIA, Fig. 4E, Fig. 5C) presented a moderate number of labeled somata, and the posteromedial and posterolateral parts of the medial BST showed a few labeled neurons (Fig. 4C, Table 2). In the rest of the BST complex,

very scarce labeling was observed in the ventral and anterior parts of the medial division, as well as in the ventral and posterior part of the lateral BST (Table 2).

Retrograde labeling in the cortex and the hippocampal formation

In the mesocortex, labeling was dense in the insular region and scarce in the prefrontal and the perirhinal regions. Thus, the agranular insular cortex (AI) displayed a dense population of cells in layer V, which was unevenly distributed. Whereas the ventral part of the AI showed dense labeling, in its dorsal part labeled cells were scarce (Table 2, Fig. 4B). Finally, the posterior AI displayed a moderate density of labeling (Table 2, Fig. 4C, D). By contrast, the prelimbic cortex, the medial orbital cortex, the dorsal peduncular cortex, the infralimbic cortex, the claustrum, the perirhinal cortex and the ectorhinal cortex displayed sparse labeled cells (Table 2, Figs. 1C and 4B-G).

Within the hippocampal formation, the density of retrograde labeling was moderate in the lateral entorhinal cortex (LEnt) (Table 2, Fig. 4F, G) and scarce in the cell layer of the ventral aspect of CA3, CA1 and subiculum (Table 2, Fig. 4G).

Retrograde labeling in the septum and basal forebrain

In general, the injections in the ACo gave rise to scarce labeling in the basal cerebral hemispheres, with exception of the septohippocampal nucleus in the septum and the nucleus of the horizontal limb of the diagonal band (HDB)/magnocellular preoptic nucleus (MCPO). Thus, a dense population of darkly stained somata was observed in the septohippocampal nucleus, where labeling was high at rostral levels, just ventral to the dorsal *tenia tecta* (Table 2) and decreased caudally (Fig. 4B). Within the diagonal band, a few labeled cells were observed in its ventral aspect, next to the olfactory tubercle (Table 2, Fig. 4B), while a moderate density of darkly stained cells were present in the HDB and MCPO. In addition, few labeled somata were observed in the medial septal nucleus (Table 2, Fig. 4B) lining up at the boundary with the intermediate part of the lateral septal nucleus.

A low density of lightly labeled cells was also present in the semilunar nucleus, the ventral pallidum and, more caudally, in the *substantia innominata* (Table 2, Fig. 4B-C). At these caudal levels (Fig. 4C), retrograde labeling was also observed in different components of the rostral extended amygdala including the interstitial nucleus of the

posterior limb of the anterior commissure and different subnuclei of the BST (see above).

Retrograde labeling in the preoptic area and the hypothalamus

Modern genoarchitecture studies have revealed that the preoptic region is part of the subpallium (Puelles and Rubenstein, 2015), and consequently we describe the results in this regions apart from the hypothalamus. Low numbers of labeled cells were present in the medial preoptic area, the medial preoptic nucleus and the anterior hypothalamic area (Table 2, Fig. 4C).

In general, in the hypothalamus retrograde labeling consisted in scattered cells in different nuclei, with the exception of the posterior hypothalamic area. Thus, low numbers of labeled cells were present in the anterior hypothalamic area (Table 2, Fig. 4C, D). Within the tuberal hypothalamus, a few labeled cells were seen in ventromedial hypothalamic nucleus and lateral hypothalamic area and very few in *tuber cinereum* (Table 2, Fig. 4D, E). In contrast, retrograde labeling was moderate in the posterior hypothalamic area (Table 2, Fig. 4F). In addition, at mamillary levels, a few cells appeared in the ventral premamillary nucleus, and even fewer cells were seen in its dorsal part and in the supramamillary nucleus (Table 2, Fig. 4F).

Retrograde labeling in the thalamic complex

After the FG injections, retrograde labeling was mainly observed in some midline nuclei of the thalamus and in the posterior intralaminar thalamic region. In the midline, a few labeled neurons were seen in the nucleus reuniens, but most of the labeling was located in the paraventricular thalamic nucleus (PV). There, the distribution of labeled cells is heterogeneous, with a moderate-to-low density in the anterior division of the nucleus and a moderate-to-high density in its posterior part (Fig. 4C-F; Table 2). At these caudal levels, there is a continuum of labeling bridging the posterior PV with the posterior intralaminar thalamus, which includes cells in the subparafascicular thalamic nucleus (SPF), the parvicellular part of SPF (SPFPC), and the posterior intralaminar thalamic nucleus (PIL) (Table 2, Fig. 4F, G and Fig. 5E). In addition, scarce labeling was present in the peripeduncular nucleus (PP), medial part of the medial geniculate nucleus (MGM) and the suprageniculate thalamic nucleus (Table 2, Fig. 4G and Fig. 5E). This

large population of labeled cells seems to extend rostrally until the prethalamic *zona incerta*, where a few labeled cells were observed (Table 2, Fig. 4D, E)

Retrograde labeling in the midbrain and brainstem

The midbrain and brainstem showed few labeled cells, with the exception of the parabrachial region where a moderately dense population of labeled cells was distributed in its lateral and medial divisions (Table 2, Figs. 4H and 5F).

In the remaining nuclei of the midbrain and brainstem, the periaqueductal gray, the ventral tegmental area (VTA), the dorsal raphe nucleus and the *locus coeruleus* showed scarce labeling (Table 2, Fig. 4G, H). Moreover, in the rostral linear nucleus of the raphe and the oral part of the pontine reticular nucleus very scarce labeled cells were present (Table 2, not shown). In addition, in the cases where small tracer deposits appeared along the micropipette tract in the caudate putamen, labeled cells were observed in the *substantia nigra* (Fig. 4F, G).

Contralateral retrograde labeling

Although the observed retrograde labeling was mostly ipsilateral to the injection sites, a few labeled cells were also present in a number of contralateral nuclei. In the olfactory system, the rostral Pir presented moderate labeling located in its layer II. A few labeled somata were also observed in the caudal Pir. The dorsal *tenia tecta* showed a very scarce number of labeled cells in its layer III. Within the amygdala, the contralateral PLCo showed scarce labeling and the PMCo and BMA very few labeled somata. In the contralateral LEnt a few labeled cells were observed. The diagonal band and the *substantia innominata* showed a few labeled cells in the contralateral hemisphere. Also in the thalamus, scarce contralateral labeling was observed in the SPF, SPFPC and PP and, to a lesser extent, the PIL, PV, and in the periventricular fiber system, nucleus reuniens and the prethalamic *zona incerta*. The hypothalamus contralateral to the injection displayed a few labeled cells as well, located in the ventromedial hypothalamic nucleus, the lateral hypothalamic area and the posterior hypothalamic area. Finally, a low number of labeled neurons was also observed contralaterally in the periaqueductal gray, VTA, rostral linear nucleus of the raphe and parabrachial nucleus.

Anterograde labeling after BDA injections into the ACo

Eight injections were located in the ACo, four of which were centered and restricted to this nucleus (cases #1243, #1245, #1335 and #1340, Fig. 3E-I). The extent of the effective injection sites was considered as the area showing an intensely dark extracellular deposit of HRP reaction product obscuring the details of the underlying tissue (see Fig 3K). In three cases #1340, #1243, #1245 the injection involved the superficial and deep layers of the ACo, whereas the injection #1335 was very small and centered in layer II at caudal levels. Two of the four injections (#1243 and #1245) presented a small deposit of tracer along the micropipette track in the BMA and dorsal anterior amygdaloid area (Fig. 3E, H). All of the restricted injections gave rise to a consistent pattern of anterograde labeling (case #1340 is illustrated in Fig. 6). In addition, other four injections were mainly located in the ACo, but involved other nuclei such as the CxA (n = 2), the BMA (n = 1) or the PLCo (n = 1). These non-restricted injections resulted in a similar pattern of labeling to that described following the restricted injections, although as expected additional fiber labeling was observed.

In general, the ACo injections gave rise to widespread projections, with the densest labeling located in some nuclei of the olfactory system, the chemosensory amygdala and, to a lesser extent, in some structures of the central extended amygdala, basal forebrain and tuberal hypothalamus.

Anterograde labeling in the olfactory system

The injections in the ACo did not give rise to anterograde labeling in the MOB. In the AOB, tracer injections affecting all layers of the nucleus (Figs. 3 and 6G) gave rise to a small amount of anterogradely labeled fibers in the AOB, present mainly in the mitral cell layer (Fig. 6A). In addition, very scarce labeling was observed in the granular cell layer of the accessory olfactory bulb (Fig. 6A).

In the olfactory structures, the Pir and the endopiriform nucleus showed the highest density of labeled fibers. Anterograde labeling in the Pir was particularly dense in its caudal part (Table 2, Fig. 6B-J), and was observed mainly in its layers I and III. In the endopiriform nucleus, fiber labeling is denser in the ventral endopiriform nucleus (Table 2, Fig. 6B-J). The tenia tecta presented moderate labeling in its ventral part, and only scarce labeling in its dorsal part. In addition, the posterior part of the anterior olfactory nucleus showed scarce labeling (Table 2, Fig. 6B). Finally, very scarce

labeling can be observed in the lateral, medial and ventral part of the anterior olfactory nucleus (Table 2, Figs. 1F and 6B).

Anterograde labeling in the amygdala

As described for retrograde labeling, the chemosensory amygdala showed the highest density of anterogradely labeled fibers, with important projections being present also to the basomedial amygdala and part of the central amygdala (see Table 2).

In the olfactory amygdala (Table 2), BDA injections gave rise to very dense anterograde labeling in the PLCo, present mainly in layer I (Figs. 1D, 6H-J and 7D). In addition, the CxA and the LOT showed a moderate level of fiber labeling (Figs. 6E-H and 7C), and the amygdalopiriform transition area displayed a scarce number of labeled fibers (Figs. 6K and 7E).

In the vomeronasal amygdala (Table 2), injections in the ACo gave rise to dense fiber labeling in the Me. The anterior Me showed a very dense presence of labeled fibers, centered in its anterodorsal aspect. The posterodorsal and posteroventral Me displayed a dense projection from ACo (Figs. 6G-I and 7D). In addition, in the dorsal and ventral parts of the anterior amygdaloid area, a very dense presence of labeled fibers was observed (Figs. 6E, F and 7C). In the BAOT (Fig. 6G) and the PMCo (Figs 6J, K and 7D) moderate fiber labeling was present.

The basolateral complex displays a very dense fiber labeling in the BMA (Fig. 6G-I) and dense labeling in BMP (Figs. 6I, J and 7D). In addition, the ventral part of the basolateral nucleus (Fig. 6I) presented a moderate level of labeled fibers. Other regions of the basolateral complex, like its anterior and posterior subnuclei, the dorsolateral part of the lateral nucleus and the amygdalohippocampal area showed scarce projections from the ACo (Figs. 6G-K and 7D).

In the central nucleus, moderate anterograde labeling appeared in its medial part, and scarce labeling was present in the capsular and lateral parts (Fig. 6G-I). In addition, very scarce levels of labeled fibers were present in the amygdalostriatal transition area (Table 2).

Anterograde labeling in the bed nucleus of the stria terminalis

The injections in the ACo resulted in moderate anterograde labeling in the BST (see Table 2). A moderately dense terminal field was observed in the BSTIA (Figs. 6H, I and 7D). The ventral part of the lateral and medial BST divisions (Figs. 6D and 7B), as well as the posterointermediate and the posteromedial aspects of the medial BST (Figs. 6E and 7C) showed a moderate presence of labeled fibers. On the other hand, the posterior (Figs. 6D, E and 7B) and dorsal (Figs. 6D and 7C) parts of the lateral BST division, as well as the anteromedial BST and the posterolateral aspect of the medial BST presented scarce labeling.

Anterograde labeling in the cortex and the hippocampal formation

In the hippocampal formation moderate anterograde labeling was present in the caudal CA1, between the *stratum lacunosum molculare* and the *stratum radiatum* (Figs. 1E, 6K and 7E). Fiber labeling was also moderate in LEnt (Fig. 6K).

Regarding the cerebral cortex, the observed labeling was scarce in the medial orbital, dorsal peduncular, perirhinal (Figs. 6B and H-K and 7E) and infralimbic cortices (Figs. 6B and 7A). In addition, very scarce levels of labeled fibers were present in the agranular insular cortex (Fig. 6B-G), the prelimbic cortex (Figs. 6B and 7A), the claustrum (Fig. 6C-G) and the ectorhinal cortex (Fig. 6H-K).

Anterograde labeling in the septum and basal forebrain

In the lateral septal complex, a low number of fibers were observed in the septohippocampal nucleus (Fig. 6C). In the remaining nuclei of the lateral septum only very scarce anterograde labeling was present (Table 2, Fig. 6C, D). In contrast, the diagonal band showed dense fiber labeling in the HDB/MCPO, located mainly in its ventral aspect (Figs. 6D-E and 7B).

Within the striato-pallidal complex, a high density of labeled fibers was observed in the *substantia innominata* (Figs. 6D-F and 7B). Dense anterograde labeling was also present in the interstitial nucleus of the posterior limb of the anterior commissure, especially in its medial subdivision (Figs. 6D-F and 7B, C), and moderate fiber labeling was observed in the semilunar nucleus and the ventral pallidum (Figs. 6C-E and 7C).

Within the ventral striatum, scarce labeling appeared in the olfactory tubercle (Figs. 6B-D and 7B), with axons mainly surrounding the islands of Calleja. Only a few fibers enter both the ventromedial and the major islands. In addition, a small number of fibers

were observed in the nucleus accumbens, both in the core and caudally in the shell (Fig. 6C).

Anterograde labeling in the preoptic area and hypothalamus

In the preoptic region, there was a moderate amount of anterograde labeling in the medial preoptic nucleus and medial preoptic area (Fig. 6C-F). In addition, scarce labeling was observed in the lateral preoptic area (Fig. 6C) and, more rostrally, in the anterior commissural nucleus. A few labeled fibers could also be found in the median preoptic nucleus and the anterodorsal preoptic nucleus (Fig. 6D, E).

In the hypothalamus, anterograde labeling appeared in many hypothalamic nuclei, although dense fiber labeling was present only in the lateral hypothalamic area (Table 2).

At anterior levels (paraventricular and supra-ventricular areas), a low density of labeled fibers was observed in the paraventricular hypothalamic nucleus, the anterior hypothalamic area, the lateroanterior hypothalamic nucleus (Fig. 6F), the suprachiasmatic nucleus and the periventricular hypothalamic nucleus (Fig. 6F, G).

In the tuberal region, a dense presence of labeled fibers was observed in the lateral hypothalamic area, mainly in the magnocellular nucleus of the lateral hypothalamus (Fig. 6H, I). In addition, moderate fiber labeling was observed in the medial tuberal nucleus and the terete hypothalamic nucleus (Fig. 6J). Finally, scarce labeled fibers were present in the retrochiasmatic area, the dorsomedial and ventromedial hypothalamic nuclei, the PH and the arcuate nucleus (Fig. 6H, I), as well as in the subthalamic nucleus, extending into the parasubthalamic nucleus.

Finally, scarce anterograde labeling was seen in the dorsal pre-mammillary nucleus and the supra-mammillary nucleus (Table 2).

Anterograde labeling in the thalamic complex

The injections in the ACo resulted in scarce, but widespread, anterograde labeling in the thalamus. Fiber labeling was moderate in the nucleus of the *stria medullaris* (Fig. 6F), and a few fibers could also be observed in the lateral habenula. In addition, scarce labeled fibers are present in several midline thalamic nuclei (nucleus reuniens, PV, central medial, mediodorsal, intermediodorsal and paratenial thalamic nuclei, Fig. 6F-J).

A few labeled axons reached the posterior intralaminar thalamic nuclei (SPFPC, PIL, PP, the supragenulate thalamic nucleus, the parafascicular thalamic nucleus, and the triangular part of the posterior thalamic nucleus, Fig. 6J, K). Finally, a few labeled fibers were present in the prethalamic *zona incerta*.

Anterograde labeling in the midbrain and brainstem

The midbrain and brainstem showed low levels of anterograde labeling, with the exception of the pedunclopontine tegmental nucleus (Fig. 6L), which displayed a moderate level of labeled fibers. There was also scarce labeling in the periaqueductal gray, where the fibers were mainly present in its lateral part (Fig. 6K), the compact part of the substantia nigra (Fig. 6K), the VTA, the lateral parabrachial nucleus and the *locus coeruleus* (Figs. 6K-M and 7E, F). Part of the labeled fibers in the substantia nigra appeared to be fibers of passage. Finally, a few labeled fibers were observed in some other midbrain (parvicellular part of the red nucleus, reticular part of the *substantia nigra*, deep mesencephalic nucleus) and brainstem structures (medial parabrachial nucleus, dorsal raphe and paramedian raphe nucleus) (Table 2).

Contralateral anterograde labeling

The anterograde labeling obtained following tracer injection in the ACo was mainly ipsilateral. However, a few fibers could be observed crossing the midline in the ventralmost part of the anterior commissure. In the contralateral telencephalon, scarce labeling was present in the VTT, the BSTMV, BSTMPM, BSTLV and BSTLP, in the diagonal band complex and in the SI. In the hypothalamus, scarce innervation appeared in the LH (at anterior and tuberal levels) and in the MCLH. Very few fibers were present in some of the midline thalamic nuclei (PVA, CM, Re and MD). Finally, in the brainstem very scarce innervation appeared in the PAG, VTA, SNC and PPTg.

DISCUSSION

The chemosensory amygdala is an evolutionary conserved part of the amygdaloid complex in vertebrates (Martínez-García et al., 2007), which plays a key role in social and sexual behavior. As part of a long-term project aiming to characterize the anatomical connections of the chemosensory amygdala, here we report a comprehensive

description of the afferent and efferent connections of the ACo in mice (see Fig. 8), for which very scarce data are available (Martínez-García et al., 2012).

Olfactory system

The results of the retrograde tracing experiments confirm that the ACo receives a major input from the main olfactory bulb, and a minor one from the accessory olfactory bulb, corroborating previous studies (Pro-Sistiaga et al., 2007; Kang et al., 2009; Cádiz-Moretti et al., 2013). Thus, the MOB provides a predominant olfactory input to the ACo, while the vomeronasal input from the AOB is less relevant, at least in anatomical terms. The retrograde labeling in the MOB and AOB following the tracer injections in the ACo was observed throughout their mitral cell layer, and therefore showed no topographic organization. These results indicate that the projections from the bulbs do not arise from particular subsets of mitral cells, but instead from large populations (maybe most of the mitral cells) probably responsive to many odorants or chemical signals. In this respect, a previous study found that Fos expression in the ACo was induced equally by a novel odor and by cat odor (Dielenberg et al., 2001). Regarding the conspecific odors, the exposure to volatiles derived from male-soiled bedding induced Fos expression in the ACo in female mice (Moncho-Bogani et al., 2005). Notably, the Fos induction in the ACo was observed equally when the male volatiles were attractive (because of previous chemosensory experience of the females) and when the male volatiles induced no attraction (in inexperienced females). Taken together, the results of these studies (Dielenberg et al., 2001; Moncho-Bogani et al., 2005) suggest that general odorants, and not only emotionally-labeled chemical cues, apparently activate the ACo. The activation by general odorants may allow the ACo to be involved in the association of olfactory cues with other stimuli.

In agreement with previous studies, the ACo does not project back to the MOB (de Olmos et al., 1978; Luskin and Price, 1983; Shipley and Adameck, 1984; Petrovich et al., 1996). However, we found a very light projection to the AOB. The fact that it has not been observed in rats may be due to its very small entity or to interspecies differences.

Our findings show that the ACo receives substantial projections arising from the olfactory cortex, a hodological feature shared with the CxA, the Me and the PMCo (Gutiérrez-Castellanos et al., 2014; Cádiz-Moretti et al., 2016a, 2016b). The ACo also

projects back to the olfactory cortex. Previous studies already showed that the olfactory cortex is reciprocally connected with the ACo (Luskin and Price, 1983; Petrovich et al., 1996; McDonald, 1998; Majak et al., 2004). The ACo receives denser projections from the caudal than from the rostral Pir, a hodological feature also showed by the Me (Cádiz-Moretti et al., 2016a). In contrast, the CxA shows the opposite pattern, receiving more projections from the rostral Pir (Cádiz-Moretti et al., 2016b). According to electrophysiological studies, the posterior Pir shows associative encoding characteristics (Calu et al., 2007), and thus may act as an associative cortex that sends to the ACo highly processed olfactory information that includes the behavioral significance of the odorant.

Connections with the amygdaloid complex and BST

The ACo receives its strongest projections from the chemosensory amygdala, and gives rise to moderate projections back to these structures. Our results showed that it receives important projections from the olfactory amygdaloid nuclei, such as the PLCo, CxA and LOT, and projects back mainly to the PLCo. The efferent projections of the LOT (Santiago and Shammah-Lagnado, 2004) and PLCo (Majak and Pitkänen, 2003, named periamygdaloid cortex by these authors) have been reported with restricted injections of anterograde tracers.

Regarding the vomeronasal amygdala, the ACo received important projections arising from the PMCo and BAOT and moderate projections from the Me and anterior amygdaloid area. Similar results were obtained with anterograde injections in the PMCo (Canteras et al., 1992; Gutiérrez-Castellanos et al., 2014) and Me (Canteras et al., 1995; Pardo-Bellver et al., 2012), with minor differences regarding the density of the anterograde labeling observed in ACo. The projections from the ACo back to the vomeronasal amygdala are relatively lighter, with the exception of the projection to the medial nucleus, in agreement with previous results (Petrovich et al., 1996; Cádiz-Moretti et al., 2016a). The projection from the ACo to the Me has been proposed to be the substrate allowing the association of olfactory and vomeronasal stimuli (Keshavarzi et al., 2015; see Guthman and Vera, 2016).

In summary, the ACo is reciprocally connected with both the olfactory and vomeronasal nuclei, similar to the situation reported for the Me and PMCo. Therefore, although the ACo receives a predominant olfactory input from the MOB, its bidirectional

connections with the secondary centers within the chemosensory amygdala allow further integration of olfactory and vomeronasal information.

Concerning the deep amygdaloid nuclei, the ACo received moderate projections from the basomedial nucleus and minor projections arising from the basolateral, lateral and central amygdaloid nuclei (Table 2). These results are consistent with previous findings (for the lateral amygdala, Pitkänen et al., 1995; for the basolateral nucleus, Savander et al., 1995). With regard to the basomedial nucleus, consistent with our results Petrovich et al. (1996) described a dense projection from the BMA to ACo, while the BMP originated only a sparse input. Savander et al. (1996) found similar results (see their figures 3 and 5), although they described the basomedial projections to the ACo as light in general. The projections back to the basomedial nucleus are quite dense (Petrovich et al., 1996), while the projections to the lateral and basolateral nuclei are very light. The ACo gives also rise to a moderate projection to the medial part of the central nucleus, described also in rats (Petrovich et al., 1996; Savander et al., 1996). Therefore, ACo is reciprocally connected with the basomedial nucleus, which has been recently shown to be involved in controlling fear and anxiety (Adhikari et al., 2015) and social stress (Mesquita et al., 2016). Moreover, the ACo projects directly to the medial central nucleus, which is a key structure in activating the fear responses (Ehrlich et al., 2009). This connectivity strongly suggests its involvement in processing emotional information (Fig. 8).

Regarding the BTS complex, the ACo receives projections mainly arising from the BSTMPI and the BSTIA. The projections back to the BST are more important, innervating most of the complex. These findings are in agreement with previous studies reported in rats (Dong and Swanson, 2004, 2006a, 2006b), although the efferent projections to the anterior subdivisions to the BST appeared somewhat lighter in rats (Petrovich et al., 1996). The projection to the anterior BST is consistent with innervation of the central amygdala described above, since these structures form the central extended amygdala (Martínez-García et al., 2012). The reciprocal connections with the posterior BST (and the medial amygdala) indicate that the ACo modulates the network of sexually dimorphic, steroid-sensitive structures involved in the control of sociosexual behaviors (Newman, 1999; Otero-García et al., 2014).

Connections with the cortex and hippocampal formation

The results of the present work show minor connections of the cerebral cortex with the ACo, with the exception of some prefrontal regions and the AI. The connections with the agranular insular cortex have been previously described in rats with anterograde (McDonald et al., 1996; Shi and Cassell, 1998; Luskin and Price, 1983) and retrograde tracers (Haberly and Price, 1978; Ottersen, 1982). The input from the AI is shared with the Me. Therefore, the ACo and the Me, which are multimodal structures as indicated by the whole pattern of afferents, receive a common input from the AI. The AI receives convergent projections from the gustatory and viscerosensory areas of the dysgranular and granular insular cortex and from the Pir (Shi and Cassell, 1998). In addition, it is connected with the gustatory thalamic nucleus. Therefore, the projections arising from the ventral and posterior AI may be modulating olfactory information processing in the ACo, placing the odor in a gustatory and viscerosensory context.

Besides the afferent projections from the AI, the ACo receives minor projections arising from the prefrontal cortex (infralimbic and prelimbic areas), as previously reported in rats (Hurley et al., 1991; Takagishi and Chiba, 1991; McDonald et al., 1996; Shi and Cassell, 1998).

The ventral part of the hippocampus shows light reciprocal connections with the ACo, as well as with the Me (see Cádiz-Moretti et al., 2016a) and the PMCo (Gutiérrez-Castellanos et al., 2014). Therefore, on anatomical grounds the ventral hippocampus can influence neural processing in the chemosensory amygdala.

Connections with the septum and basal forebrain

The basal forebrain projection to the ACo is a common trait of the corticomедial amygdaloid nuclei (Ottersen, 1980; Martínez-García et al., 2012). However, the projections to the LOT (Grove, 1988) and the CxA (Cádiz-Moretti et al., 2016b) arise in the cholinergic neurons of the basal forebrain. In contrast, the ACo does not show cholinergic innervation, suggesting that the basal forebrain input originates in non-cholinergic (probably GABAergic) neurons (Semba, 2000). A similar projection from the basal forebrain innervates also the Me (Cádiz-Moretti et al., 2016a) and the PMCo (Gutiérrez-Castellanos et al., 2014), which is probably non-cholinergic according to the negative reaction of these structures to the AchE histochemistry (Paxinos and Franklin 2004). The ACo gives rise to a moderate projection back to the basal forebrain,

targeting mainly the diagonal band and the *substantia innominata*, and to a minor extent the olfactory tubercle (Novejarque et al., 2011).

Connections with the hypothalamus

The hypothalamus is considered an essential interface between the endocrine, autonomic and somatomotor systems (Simerly, 2015). Within the variety of behaviors in which the hypothalamus is involved, it regulates aggressive-defensive responses and the expression of appropriate sexual and maternal behaviors (Simerly, 2015). In rodents, the expression of these behaviors depends largely on the chemosensory systems (Martínez-García et al., 2009; Baum and Cherry, 2015). The efferent projections from the ACo to the hypothalamus are relatively light, with the exception of a number of structures of the lateral hypothalamus, especially at tuberal levels. This pattern of projections is consistent with previous descriptions (Price et al., 1991; Petrovich et al., 1996; Niu et al., 2012). The hypothalamic targets of the ACo include the ‘hypothalamic aggression area’ (Toth et al., 2010), located in the mediobasal hypothalamus lateral to the ventromedial hypothalamic nucleus. Thus, the ACo may be involved in initiating aggressive responses towards conspecifics, which are known to be elicited by chemical cues (Chamero et al., 2007; Martín-Sánchez et al., 2015). In fact, maternal aggression in lactating female mice has been shown to induce Fos expression in the ACo (Gammie and Nelson, 2001).

It is also possible that the projections from the ACo to the lateral hypothalamus reach the neurons projecting to the preganglionic neurons of the spinal cord (Saper, 1995), which in turn innervate the sympathetic neurons of the superior cervical ganglion controlling the vomeronasal pumping mechanism (Meredith and O’Connell, 1979). This circuit has been proposed to mediate olfactory-elicited vomeronasal pumping (Martínez-Marcos et al., 2002).

Connections with the thalamus

Our results showed that the thalamus send important projections to ACo from the posterior intralaminar complex, and minor projections arising from the paraventricular thalamus and the nucleus reuniens. The ACo sends back moderate projections to the thalamus, which innervate several midline thalamic nucleus (Fig. 8).

The projections arising from the paraventricular thalamus and the nucleus reuniens were previously described in rats (Moga et al., 1995; Turner and Herkenham, 1991; Vertes et al., 2006). The paraventricular thalamic nucleus has recently been shown to be involved in the expression of learned fear in an auditory fear conditioning paradigm (Li et al., 2014). Since electrophysiological evidence implicate the ACo in olfactory fear conditioning (Sevelinges et al., 2004), it may be possible that the PV projection to the ACo play a role in the expression of fear to olfactory stimuli.

Regarding the posterior intralaminar complex of the thalamus, the SPF, SPFPC and PIL showed important projections to the ACo, while the MGM, PP and suprageniculate nucleus sent minor projections. The projections arising from the MGM and PIL to the ACo have been previously reported (Turner and Herkenham, 1991; LeDoux et al., 1985). These structures (MGM and PIL) receive auditory and somatosensory inputs (LeDoux et al., 1987), and contain tone-responding and somatosensory-responding neurons (Bordi and LeDoux, 1994). Moreover, electrical stimulation of the PIL/MGM area functions as an effective unconditioned stimulus inducing fear learning (Cruikshank et al., 1992). Therefore, consistent with the electrophysiological data showing that the ACo plays a role in olfactory fear conditioning (Sevelinges et al., 2004), it receives olfactory information from the olfactory bulb (as well as from the Pir) and somatosensory information from the posterior intralaminar thalamus, making it a good candidate to be involved in this kind of learning.

In addition to footshock-related somatosensory information relayed by some posterior intralaminar nuclei, genital somatosensory information has been proposed to reach the SPFPC (the medial aspect of the posterior intralaminar thalamus). In fact, Fos studies have shown that this nucleus is activated in male hamsters when mating to ejaculation (Coolen et al., 1997). Therefore, the thalamic projection to ACo may relay both aversive and appetitive aspects of somatosensory information.

Connections with the midbrain and brainstem

The brainstem and midbrain showed minor projection to and from the ACo, with the parabrachial nucleus being the structure with somewhat denser afferent projections.

The afferent projections from the parabrachial nucleus to the ACo have been previously reported in rats (Bernard et al., 1993). The parabrachial nucleus also projects to the Me

(Cádiz-Moretti et al., 2016a) and to the central and basolateral complex (Bernard et al., 1993). The parabrachial nucleus has been shown to integrate taste and visceral sensory information in the context of taste aversion learning (Yamamoto et al., 1994). Therefore, the reciprocal connection between the parabrachial nucleus and the ACo may relate taste and viscerosensory information to incoming olfactory information.

The connectivity of the ACo compared with that of the adjacent structures (CxA, Me and BMA)

The ACo limits laterally with the CxA and medially with the Me, and has an its inner diffuse boundary with the BMA. The connectivity pattern of each one of these structures shows both similarities and differences with that of the ACo.

The laterally adjacent CxA shows a restricted pattern of (mainly intratelencephalic) afferent projections, originated mainly by the olfactory system and the basal forebrain (Cádiz-Moretti et al., 2016b). It lacks the thalamic input shown by the ACo. The ACo, in contrast, does not receive the cholinergic input from the basal forebrain that is one of the defining features of the CxA. Regarding the efferent projections, the CxA gives rise to very dense projections to the basolateral amygdaloid nucleus, which receives only minor projections from ACo. In addition, the CxA projections to the thalamus, midbrain and brainstem are very small, whereas the projections from the ACo to these brain regions, although light in general, are much more extensive (Cádiz-Moretti et al., 2016b).

Medially, the ACo limits with the anterior Me. Compared to the ACo, the anterior Me shows much stronger interconnections with the vomeronasal system (AOB, BAOT, PMCo and posteromedial BST) (Cádiz-Moretti et al., 2016a) and gives rise to a dense projection to the ventromedial hypothalamus (Pardo-Bellver et al., 2012).

The most diffuse boundary of the ACo is that with the BMA, which is located deep to it. In fact, from the developmental point of view the neurons of the BMA and the ACo probably originate in the same region of the neuroepithelium (Martínez-García et al., 2012). Compared with the connections of the ACo, the BMA projects more strongly to the nucleus accumbens (Novejarque et al., 2011) and to the central amygdala (Petrovich et al., 1996; our unpublished observations in mice). Regarding the afferent projections to the BMA, there are no studies focused on these projections in mice, but in rats the

BMA receives a strong intraamygdaloid projection from the lateral nucleus (Pitkänen et al., 1995), which is lacking in the case of the ACo. In addition, the BMA is strongly interconnected with the hippocampal and parahippocampal formations (Pitkänen et al., 2000), whereas the ACo shows only light interconnections with these structures. Finally, the BMA lacks connections with the midbrain and brainstem (Pitkänen, 2000), which are quite extensive (although relatively light) in the case of the ACo.

Functional remarks

In spite of the described differences, the set of afferent projections described for the ACo is, to some extent, similar to that of the medially adjacent Me (Cádiz-Moretti et al., 2016a) and (taken as a whole) quite different from those of the laterally adjacent CxA (Cádiz-Moretti et al., 2016b). In fact, the thalamic projections to the ACo and Me are very similar, in particular those originated by the posterior intralaminar thalamic nuclei. This thalamic input, together with the afferents arising from the brainstem, suggest that taste, viscerosensory, somatosensory and nociceptive information can reach the ACo, and consequently it may be involved in a broad number of behaviors. Previous studies using Fos as an activity marker have shown activation of the ACo in both aversive and appetitive motivated tasks (Knapska et al., 2007). Thus, it seems that the ACo may play a role in most emotional behaviors as long as there is relevant olfactory information involved. The set of efferent projections of the ACo differs from the pattern described for the Me, especially regarding the projections to the central extended amygdala and the lateral hypothalamus. These specific outputs suggest a role in activating defensive and/or aggressive responses.

ACKNOWLEDGEMENTS

The authors are grateful to Carmen Agustín-Pavón for reading and commenting on the manuscript, and to Adoración Hernández-Martínez for technical assistance.

CONFLICT OF INTEREST STATEMENT

The authors declare no conflict of interest.

AUTHOR'S ROLE

EL, FM-G and BC-M designed the study. BC-M and MA-A performed the experiments. BC-M, MA-A and CP-B analyzed and interpreted data. BC-M, MA-A and EL prepared the manuscript draft. EL and FM-G supervised the study, critically revised the manuscript and obtained funding.

REFERENCES

- Adhikari, A., Lerner, T. N., Finkelstein, J., Pak, S., Jennings, J. H., Davidson, T. J., ... Deisseroth, K. (2015). Basomedial amygdala mediates top-down control of anxiety and fear. *Nature*, *527*, 179–185. <https://doi.org/10.1038/nature15698>
- Baum, M. J., & Cherry, J. A. (2015). Processing by the main olfactory system of chemosignals that facilitate mammalian reproduction. *Hormones and Behavior*. <https://doi.org/10.1016/j.yhbeh.2014.06.003>
- Bernard, J. F., Alden, M., & Besson, J. M. (1993). The organization of the efferent projections from the pontine parabrachial area to the amygdaloid complex: A phaseolus vulgaris leucoagglutinin (PHA-L) study in the rat. *Journal of Comparative Neurology*, *329*(2), 201–229. <https://doi.org/10.1002/cne.903290205>
- Bordi, F., & LeDoux, J. E. (1994). Response properties of single units in areas of rat auditory thalamus that project to the amygdala - II. Cells receiving convergent auditory and somatosensory inputs and cells antidromically activated by amygdala stimulation. *Experimental Brain Research*, *98*(2), 275–286. <https://doi.org/10.1007/BF00228415>
- Brock, O., Keller, M., Douhard, Q., & Bakker, J. (2012). Female mice deficient in Alpha-Fetoprotein show female-typical neural responses to conspecific-derived pheromones. *PLoS ONE*, *7*(6). <https://doi.org/10.1371/journal.pone.0039204>
- Bupesh, M., Legaz, I., Abellán, A., & Medina, L. (2011). Multiple telencephalic and extratelencephalic embryonic domains contribute neurons to the medial extended amygdala. *Journal of Comparative Neurology*, *519*(8), 1505–1525. <https://doi.org/10.1002/cne.22581>
- Cádiz-Moretti, B., Martínez-García, F., & Lanuza, E. (2013). Neural substrate to associate odorants and pheromones: Convergence of projections from the main and accessory olfactory bulbs in mice. In *Chemical Signals in Vertebrates 12* (pp. 3–16). New York, NY: Springer Science. <https://doi.org/10.1007/9781461459279>
- Cádiz-Moretti, B., Otero-García, M., Martínez-García, F., & Lanuza, E. (2016a). Afferent projections to the different medial amygdala subdivisions: a retrograde tracing study in the mouse. *Brain Structure and Function*, *221*(2), 1033–1065. <https://doi.org/10.1007/s00429-014-0954-y>
- Cádiz-Moretti, B., Abellán-Álvaro, M., Pardo-Bellver, C., Martínez-García, F., & Lanuza, E. (2016b). Afferent and efferent connections of the cortex-amygdala transition zone in mice. *Frontiers in Neuroanatomy*, *10*, 125. <https://doi.org/10.3389/fnana.2016.00125>
- Calu, D. J., Roesch, M. R., Stalnaker, T. A., & Schoenbaum, G. (2007). Associative encoding in posterior piriform cortex during odor discrimination and reversal

- learning. *Cerebral Cortex*, 17(6), 1342–1349. <https://doi.org/10.1093/cercor/bhl045>
- Canteras, N. S., Simerly, R. B., & Swanson, L. W. (1992). Connections of the posterior nucleus of the amygdala. *Journal of Comparative Neurology*, 324(2), 143–179. <https://doi.org/10.1002/cne.903240203>
- Canteras, N. S., Simerly, R. B., & Swanson, L. W. (1995). Organization of projections from the medial nucleus of the amygdala: a PHAL study in the rat. *Journal of Comparative Neurology*, 360(2), 213–45. Retrieved from <http://www.ncbi.nlm.nih.gov/pubmed/8522644>
- Chamero, P., Marton, T. F., Logan, D. W., Flanagan, K., Cruz, J. R., Saghatelian, A., ... Stowers, L. (2007). Identification of protein pheromones that promote aggressive behaviour. *Nature*, 450(7171), 899–902. <https://doi.org/10.1038/nature05997>
- Chapuis, J., Cohen, Y., He, X., Zhang, Z., Jin, S., Xu, F., & Wilson, D. A. (2013). Lateral entorhinal modulation of piriform cortical activity and fine odor discrimination. *The Journal of Neuroscience*, 33(33), 13449–13459. <https://doi.org/10.1523/JNEUROSCI.1387-13.2013>
- Coolen, L. M., Peters, H. J. P. W., & Veening, J. G. (1997). Distribution of Fos immunoreactivity following mating versus anogenital investigation in the male rat brain. *Neuroscience*, 77(4), 1151–1161. [https://doi.org/10.1016/S0306-4522\(96\)00542-8](https://doi.org/10.1016/S0306-4522(96)00542-8)
- Cousens, G., & Otto, T. (1998). Both pre- and posttraining excitotoxic lesions of the basolateral amygdala abolish the expression of olfactory and contextual fear conditioning. *Behavioral Neuroscience*, 112(5), 1092–1103. <https://doi.org/10.1037/0735-7044.112.5.1092>
- Cruikshank, S. J., Edeline, J. M., & Weinberger, N. M. (1992). Stimulation at a site of auditory-somatosensory convergence in the medial geniculate nucleus is an effective unconditioned stimulus for fear conditioning. *Behavioral Neuroscience*, 106(3), 471–483. Retrieved from <http://www.ncbi.nlm.nih.gov/pubmed/1616614>
- de Olmos, J., Hardy, H., & Heimer, L. (1978). The afferent connections of the main and the accessory olfactory bulb formations in the rat: An experimental HRP-study. *Journal of Comparative Neurology*, 181(2), 213–244. <https://doi.org/10.1002/cne.901810202>
- Dielenberg, R. A., Hunt, G. E., & McGregor, I. S. (2001). “When a rat smells a cat”: The distribution of Fos immunoreactivity in rat brain following exposure to a predatory odor. *Neuroscience*, 104(4), 1085–1097. [https://doi.org/10.1016/S0306-4522\(01\)00150-6](https://doi.org/10.1016/S0306-4522(01)00150-6)
- Dong, H. W., & Swanson, L. W. (2004). Projections from bed nuclei of the stria terminalis, posterior division: Implications for cerebral hemisphere regulation of defensive and reproductive behaviors. *Journal of Comparative Neurology*, 471(4), 396–433. <https://doi.org/10.1002/cne.20002>
- Dong, H. W., & Swanson, L. W. (2006a). Projections from bed nuclei of the stria terminalis, dorsomedial nucleus: Implications for cerebral hemisphere integration of neuroendocrine, autonomic, and drinking responses. *Journal of Comparative Neurology*, 494(1), 75–107. <https://doi.org/10.1002/cne.20790>
- Dong, H. W., & Swanson, L. W. (2006b). Projections from bed nuclei of the stria terminalis, anteromedial area: Cerebral hemisphere integration of neuroendocrine,

- autonomic, and behavioral aspects of energy balance. *Journal of Comparative Neurology*, 494(1), 142–178. <https://doi.org/10.1002/cne.20788>
- Ehrlich, I., Humeau, Y., Grenier, F., Cioocchi, S., Herry, C., & Lüthi, A. (2009). Amygdala Inhibitory Circuits and the Control of Fear Memory. *Neuron*. <https://doi.org/10.1016/j.neuron.2009.05.026>
- Gammie, S. C., & Nelson, R. J. (2001). cFOS and pCREB activation and maternal aggression in mice. *Brain Research*, 898(2), 232–241. [https://doi.org/10.1016/S0006-8993\(01\)02189-8](https://doi.org/10.1016/S0006-8993(01)02189-8)
- Geneser-Jensen, F. A., & Blackstad, T. W. (1971). Distribution of acetyl cholinesterase in the hippocampal region of the guinea pig. I. Entorhinal area, parasubiculum, and presubiculum. *Zeitschrift Fur Zellforschung Und Mikroskopische Anatomie (Vienna, Austria : 1948)*, 114(4), 460–81.
- Grove, E. A. (1988). Efferent connections of the substantia innominata in the rat. *Journal of Comparative Neurology*, 277(3), 347–364. <https://doi.org/10.1002/cne.902770303>
- Guthman, E. M., & Vera, X. J. (2016). A cellular mechanism for main and accessory olfactory integration at the medial amygdala. *Journal of Neuroscience*, 36(7), 2083–2085. <https://doi.org/10.1523/JNEUROSCI.4304-15.2016>
- Gutiérrez-Castellanos, N., Martínez-Marcos, A., Martínez-García, F., & Lanuza, E. (2010). Chemosensory function of the amygdala. *Vitamins and Hormones*, 83(10), 165–96. [https://doi.org/10.1016/S0083-6729\(10\)83007-9](https://doi.org/10.1016/S0083-6729(10)83007-9)
- Gutiérrez-Castellanos, N., Pardo-Bellver, C., Martínez-García, F., & Lanuza, E. (2014). The vomeronasal cortex - afferent and efferent projections of the posteromedial cortical nucleus of the amygdala in mice. *European Journal of Neuroscience*, 39(1), 141–158. <https://doi.org/10.1111/ejn.12393>
- Haberly, L. B., & Price, J. L. (1978). Association and commissural fiber systems of the olfactory cortex of the rat. I. Systems originating in the piriform cortex and adjacent areas. *Journal of Comparative Neurology*, 178(4), 711–740. <https://doi.org/10.1002/cne.901780408>
- Hurley, K. M., Herbert, H., Moga, M. M., & Saper, C. B. (1991). Efferent projections of the infralimbic cortex of the rat. *Journal of Comparative Neurology*, 308(2), 249–276. <https://doi.org/10.1002/cne.903080210>
- Janak, P. H., & Tye, K. M. (2015). From circuits to behaviour in the amygdala. *Nature*, 517, 284–292. <https://doi.org/10.1038/nature14188>
- Kang, N., Baum, M. J., & Cherry, J. A. (2009). A direct main olfactory bulb projection to the “vomeronasal” amygdala in female mice selectively responds to volatile pheromones from males. *European Journal of Neuroscience*, 29(3), 624–634. <https://doi.org/10.1111/j.1460-9568.2009.06638.x>
- Kemppainen, S., Jalkkonen, E., & Pitkänen, A. (2002). Projections from the posterior cortical nucleus of the amygdala to the hippocampal formation and parahippocampal region in rat. *Hippocampus*, 12, 735–755. <https://doi.org/10.1002/hipo.10020>
- Keshavarzi, S., Power, J. M., Albers, E. H. H., Sullivan, R. K. S., & Sah, P. (2015). Dendritic organization of olfactory inputs to medial amygdala neurons. *The Journal of Neuroscience*, 35(38), 13020–13028. <https://doi.org/10.1523/JNEUROSCI.0627-15.2015>

- Kevetter, G. A., & Winans, S. S. (1981). Connections of the corticomедial amygdala in the golden hamster. II. Efferents of the "olfactory amygdala" *The Journal of Comparative Neurology*, *197*(1), 99–111. <https://doi.org/10.1002/cne.901970108>
- Knapska, E., Radwanska, K., Werka, T., & Kaczmarek, L. (2007). Functional internal complexity of amygdala: focus on gene activity mapping after behavioral training and drugs of abuse. *Physiological Reviews*, *87*(4), 1113–1173. <https://doi.org/10.1152/physrev.00037.2006>
- Krettek, J. E., & Price, J. L. (1977). Projections from the amygdaloid complex to the cerebral cortex and thalamus in the rat and cat. *Journal of Comparative Neurology*, *172*(4), 687–722. <https://doi.org/10.1002/cne.901720408>
- LeDoux, J. E., Ruggiero, D. A., & Reis, D. J. (1985). Projections to the subcortical forebrain from anatomically defined regions of the medial geniculate body in the rat. *Journal of Comparative Neurology*, *242*(2), 182–213. <https://doi.org/10.1002/cne.902420204>
- Ledoux, J. E., Ruggiero, D. A., Forest, R., Stornetta, R., & Reis, D. J. (1987). Topographic organization of convergent projections to the thalamus from the inferior colliculus and spinal cord in the rat. *The Journal of Comparative Neurology*, *264*(1), 123–46. <https://doi.org/10.1002/cne.902640110>
- Lehman, M. N., Winans, S. S., & Powers, J. B. (1980). Medial nucleus of the amygdala mediates chemosensory control of male hamster sexual behavior. *Science*, *210*(4469), 557–560. <https://doi.org/10.1126/science.7423209>
- Li, Y., Dong, X., Li, S., & Kirouac, G. J. (2014). Lesions of the posterior paraventricular nucleus of the thalamus attenuate fear expression. *Frontiers in Behavioral Neuroscience*, *8*, 94. <https://doi.org/10.3389/fnbeh.2014.00094>
- Luskin, M. B., & Price, J. L. (1983). The topographic organization of associational fibers of the olfactory system in the rat, including centrifugal fibers to the olfactory bulb. *The Journal of Comparative Neurology*, *216*, 264–291. <https://doi.org/10.1002/cne.902160305>
- Majak, K., & Pitkänen, A. (2003). Projections from the periamygdaloid cortex to the amygdaloid complex, the hippocampal formation, and the parahippocampal region: A PHA-L study in the rat. *Hippocampus*, *13*(8), 922–942. <https://doi.org/10.1002/hipo.10134>
- Majak, K., Rönkkö, S., Kempainen, S., & Pitkänen, A. (2004). Projections from the amygdaloid complex to the piriform cortex: A PHA-L study in the rat. *Journal of Comparative Neurology*, *476*(4), 414–428. <https://doi.org/10.1002/cne.20233>
- Majkutewicz, I., Cecot, T., Jerzemowska, G., Myślińska, D., Plucińska, K., Trojnar, W., & Wrona, D. (2010). Lesion of the ventral tegmental area amplifies stimulation-induced Fos expression in the rat brain. *Brain Research*, *1320*, 95–105. <https://doi.org/10.1016/j.brainres.2010.01.009>
- Martel, K. L., & Baum, M. J. (2009). A centrifugal pathway to the mouse accessory olfactory bulb from the medial amygdala conveys gender-specific volatile pheromonal signals. *European Journal of Neuroscience*, *29*(2), 368–376. <https://doi.org/10.1111/j.1460-9568.2008.06564.x>
- Martín-Sánchez, A., McLean, L., Beynon, R. J., Hurst, J. L., Ayala, G., Lanuza, E., & Martínez-García, F. (2015). From sexual attraction to maternal aggression: when pheromones change their behavioural significance. *Hormones and Behavior* *68*,

- 65-76. <https://doi.org/10.1016/j.yhbeh.2014.08.007>
- Martínez-García, F., Novejarque, A., & Lanuza, E. (2007). Evolution of the amygdala in vertebrates. In J. H. Kass (Ed.), *Evolution of Nervous Systems* (Vol. 2, pp. 255–334). Oxford: Academic Press. <https://doi.org/10.1016/B0-12-370878-8/00139-7>
- Martínez-García, F., Martínez-Ricós, J., Agustín-Pavón, C., Martínez-Hernández, J., Novejarque, A., & Lanuza, E. (2009). Refining the dual olfactory hypothesis: pheromone reward and odour experience. *Behavioural Brain Research*, *200*(2), 277–286. <https://doi.org/10.1016/j.bbr.2008.10.002>
- Martínez-García, F., Novejarque, A., Gutiérrez-Castellanos, N., & Lanuza, E. (2012). Piriform Cortex and Amygdala. In G. Paxinos (Ed.), *The Mouse Nervous System* (pp. 140–172). San Diego, CA: Academic Press. <https://doi.org/10.1016/B978-0-12-369497-3.10006-8>
- Martínez-Marcos, A., Lanuza, E., & Halpern, M. (2002). Neural substrates for processing chemosensory information in snakes. *Brain Research Bulletin*, *57*(3–4), 543–546. [https://doi.org/10.1016/S0361-9230\(01\)00686-4](https://doi.org/10.1016/S0361-9230(01)00686-4)
- McDonald, A. J. (1998). Cortical pathways to the mammalian amygdala. *Progress in Neurobiology*, *55*(3), 257–332. [https://doi.org/10.1016/S0301-0082\(98\)00003-3](https://doi.org/10.1016/S0301-0082(98)00003-3)
- McDonald, A. J., & Mascagni, F. (1997). Projections of the lateral entorhinal cortex to the amygdala: A *Phaseolus vulgaris* leucoagglutinin study in the rat. *Neuroscience*, *77*(2), 445–459. [https://doi.org/10.1016/S0306-4522\(96\)00478-2](https://doi.org/10.1016/S0306-4522(96)00478-2)
- McDonald, A. J., Mascagni, F., & Guo, L. (1996). Projections of the medial and lateral prefrontal cortices to the amygdala: A *Phaseolus vulgaris* leucoagglutinin study in the rat. *Neuroscience*, *71*(1), 55–75. [https://doi.org/10.1016/0306-4522\(95\)00417-3](https://doi.org/10.1016/0306-4522(95)00417-3)
- Meredith, M., & O'Connell, R. J. (1979). Efferent control of stimulus access to the hamster vomeronasal organ. *The Journal of Physiology*, *286*(1), 301–316. <https://doi.org/10.1113/jphysiol.1979.sp012620>
- Mesquita, L. T., Abreu, A. R., de Abreu, A. R., de Souza, A. A., de Noronha, S. R., Silva, F. C., ... de Menezes, R. C. (2016). New insights on amygdala: Basomedial amygdala regulates the physiological response to social novelty. *Neuroscience*, *330*, 181–190. <https://doi.org/10.1016/j.neuroscience.2016.05.053>
- Moga, M. M., Weis, R. P., & Moore, R. Y. (1995). Efferent projections of the paraventricular thalamic nucleus in the rat. *Journal of Comparative Neurology*, *359*(2), 221–238. <https://doi.org/10.1002/cne.903590204>
- Moncho-Bogani, J., Martínez-García, F., Novejarque, A., & Lanuza, E. (2005). Attraction to sexual pheromones and associated odorants in female mice involves activation of the reward system and basolateral amygdala. *European Journal of Neuroscience*, *21*(8), 2186–2198. <https://doi.org/10.1111/j.1460-9568.2005.04036.x>
- Niu, J. G., Yokota S, Tsumori T, Oka T, Yasui, Y. (2012). Projections from the anterior basomedial and anterior cortical amygdaloid nuclei to melanin-concentrating hormone-containing neurons in the lateral hypothalamus of the rat. *Brain Research*, *1479*, (31-43). <https://doi.org/10.1016/j.brainres.2012.08.011>
- Newman, S. W. (1999). The medial extended amygdala in male reproductive behavior. A node in the mammalian social behavior network. *Annals of the New York Academy of Sciences* *877*, 242–257. <https://doi.org/10.1111/j.1749->

6632.1999.tb09271.x

- Novejarque, A., Gutiérrez-Castellanos, N., Lanuza, E., & Martínez-García, F. (2011). Amygdaloid projections to the ventral striatum in mice: direct and indirect chemosensory inputs to the brain reward system. *Frontiers in Neuroanatomy*, *5*, 54. <https://doi.org/10.3389/fnana.2011.00054>
- Otero-García, M., Martín-Sánchez, A., Fortes-Marco, Ll., Martínez-Ricós, J., Agustín-Pavón, C., Lanuza, E., & Martínez-García, F. (2014). Extending the socio-sexual brain: Arginine-vasopressin immunoreactive circuits in the telencephalon of mice. *Brain Structure and Function*, *219*(3), 1055–1081. <https://doi.org/10.1007/s00429-013-0553-3>
- Ottersen, O. P. (1980). Afferent connections to the amygdaloid complex of the rat and cat: II. Afferents from the hypothalamus and the basal telencephalon. *Journal of Comparative Neurology*, *194*(1), 267–289. <https://doi.org/10.1002/cne.901940113>
- Ottersen, O. P. (1982). Connections of the amygdala of the rat. IV: Corticoamygdaloid and intraamygdaloid connections as studied with axonal transport of horseradish peroxidase. *The Journal of Comparative Neurology* *205*, 30–48. <https://doi.org/10.1002/cne.902050104>
- Ottersen, O. P., & Ben-Ari, Y. (1979). Afferent connections to the amygdaloid complex of the rat and cat. I. Projections from the thalamus. *Journal of Comparative Neurology*, *187*(2), 401–424. <https://doi.org/10.1002/cne.901870209>
- Pardo-Bellver, C., Cádiz-Moretti, B., Novejarque, A., Martínez-García, F., & Lanuza, E. (2012). Differential efferent projections of the anterior, posteroventral, and posterodorsal subdivisions of the medial amygdala in mice. *Front Neuroanat*, *6*, 33. <https://doi.org/10.3389/fnana.2012.00033>
- Paxinos, G., & Franklin, K. B. J. (2004). *The mouse brain in stereotaxic coordinates*. San Diego, CA: Elsevier Academic Press.
- Petrovich, G. D., Risold, P. Y., & Swanson, L. W. (1996). Organization of projections from the basomedial nucleus of the amygdala: A PHAL study in the rat. *Journal of Comparative Neurology*, *374*(3), 387–420. [https://doi.org/10.1002/\(SICI\)1096-9861\(19961021\)374:3<387::AID-CNE6>3.0.CO;2-Y](https://doi.org/10.1002/(SICI)1096-9861(19961021)374:3<387::AID-CNE6>3.0.CO;2-Y)
- Pitkänen, A. (2000). Connectivity of the rat amygdaloid complex. In J. P. Aggleton (Ed.) *The amygdala: A functional analysis*, 2nd ed. (pp. 31–115). Oxford: Oxford University Press.
- Pitkänen, A., Pikkarainen, M., Nurminen, N., & Ylinen, A. (2000). Reciprocal connections between the amygdala and the hippocampal formation, perirhinal cortex, and postrhinal cortex in rat. A review. *Annals of the New York Academy of Sciences*, *911*(1), 369–391. <https://doi.org/10.1111/j.1749-6632.2000.tb06738.x>
- Pitkänen, A., Stefanacci, L., Farb, C. R., Go, G.-G., Ledoux, J. E., & Amaral, D. G. (1995). Intrinsic connections of the rat amygdaloid complex: Projections originating in the lateral nucleus. *Journal of Comparative Neurology*, *356*(2), 288–310. <https://doi.org/10.1002/cne.903560211>
- Price, J. L., Slotnick, B. M., & Revial, M. F. (1991). Olfactory projections to the hypothalamus. *Journal of Comparative Neurology*, *306*(3), 447–461. <https://doi.org/10.1002/cne.903060309>
- Pro-Sistiaga, P., Mohedano-Moriano, A., Ubeda-Bañon, I., Del Mar Arroyo-Jimenez, M., Marcos, P., Artacho-Pérula, E., ... Martínez-Marcos, A. (2007). Convergence

- of olfactory and vomeronasal projections in the rat basal telencephalon. *Journal of Comparative Neurology*, 504(4), 346–362. <https://doi.org/10.1002/cne.21455>
- Puelles, L., & Rubenstein, J. L. R. (2015). A new scenario of hypothalamic organization: rationale of new hypotheses introduced in the updated prosomeric model. *Frontiers in Neuroanatomy*, 9, 27. <https://doi.org/10.3389/fnana.2015.00027>
- Santiago, A. C., & Shammah-Lagnado, S. J. (2004). Efferent connections of the nucleus of the lateral olfactory tract in the rat. *Journal of Comparative Neurology*, 471(3), 314–332. <https://doi.org/10.1002/cne.20028>
- Saper C. B. (1995). The central autonomic system. In G. Paxinos (Ed.), *The Rat Nervous System* (pp. 107–135). San Diego, CA: Academic Press.
- Savander, V., Go, C.-G., Ledoux, J. E., & Pitkänen, A. (1995). Intrinsic connections of the rat amygdaloid complex: Projections originating in the basal nucleus. *Journal of Comparative Neurology*, 361(2), 345–368. <https://doi.org/10.1002/cne.903610211>
- Savander, V., Go, C.-G., Ledoux, J. E., & Pitkänen, A. (1996). Intrinsic connections of the rat amygdaloid complex: Projections originating in the accessory basal nucleus. *The Journal of Comparative Neurology*, 374(2), 291–313. [https://doi.org/10.1002/\(SICI\)1096-9861\(19961014\)374:2<291::AID-CNE10>3.0.CO;2-Y](https://doi.org/10.1002/(SICI)1096-9861(19961014)374:2<291::AID-CNE10>3.0.CO;2-Y)
- Scalia, F., & Winans, S. S. (1975). The differential projections of the olfactory bulb and accessory olfactory bulb in mammals. *Journal of Comparative Neurology*, 161(1), 31–55. <https://doi.org/10.1002/cne.901610105>
- Semba, K. (2000). Multiple output pathways of the basal forebrain: Organization, chemical heterogeneity, and roles in vigilance. *Behavioural Brain Research* 115, 117-141. [https://doi.org/10.1016/S0166-4328\(00\)00254-0](https://doi.org/10.1016/S0166-4328(00)00254-0)
- Sevelinges, Y., Gervais, R., Messaoudi, B., Granjon, L., & Mouly, A.-M. (2004). Olfactory fear conditioning induces field potential potentiation in rat olfactory cortex and amygdala. *Learning and Memory*, 11(6), 761–769. <https://doi.org/10.1101/lm.83604.the>
- Shi, C. J., & Cassell, M. D. (1998). Cortical, thalamic, and amygdaloid connections of the anterior and posterior insular cortices. *Journal of Comparative Neurology*, 399(4), 440–468. [https://doi.org/10.1002/\(SICI\)1096-9861\(19981005\)399:4<440::AID-CNE2>3.0.CO;2-1](https://doi.org/10.1002/(SICI)1096-9861(19981005)399:4<440::AID-CNE2>3.0.CO;2-1)
- Shiple, M. T., & Adamek, G. D. (1984). The connections of the mouse olfactory bulb: A study using orthograde and retrograde transport of wheat germ agglutinin conjugated to horseradish peroxidase. *Brain Research Bulletin*, 12(6), 669–688. [https://doi.org/10.1016/0361-9230\(84\)90148-5](https://doi.org/10.1016/0361-9230(84)90148-5)
- Simerly, R. B. (2015). Organization of the hypothalamus. In G. Paxinos G (Ed.) *The Rat Nervous System*, 4th edn. (pp 267-294). Amsterdam: Academic Press.
- Swann, J., Fabre-Nys, C., & Barton, R. (2010). Hormonal and pheromonal modulation of the extended amygdala: Implications for social behavior. In D. W. Pfaff, A. P. Arnold, S. E. Fahrbach, A. M. Etgen, & R. T. Rubin (Eds.) *Hormones, Brain and Behavior*, 2nd edn. (pp. 441–474). New York, NY: Academic Press. <https://doi.org/10.1016/B978-008088783-8.00012-7>

- Swanson, L. W., & Petrovich, G. D. (1998). What is the amygdala? *Trends in Neurosciences* 21, 323-331. [https://doi.org/10.1016/S0166-2236\(98\)01265-X](https://doi.org/10.1016/S0166-2236(98)01265-X)
- Takagishi, M., & Chiba, T. (1991). Efferent projections of the infralimbic (area 25) region of the medial prefrontal cortex in the rat: an anterograde tracer PHA-L study. *Brain Research*, 566(1-2), 26-39. [https://doi.org/10.1016/0006-8993\(91\)91677-S](https://doi.org/10.1016/0006-8993(91)91677-S)
- Toth, M., Fuzesi, T., Halasz, J., Tulogdi, A., & Haller, J. (2010). Neural inputs of the hypothalamic “aggression area” in the rat. *Behavioural Brain Research*, 215(1), 7-20. <https://doi.org/10.1016/j.bbr.2010.05.050>
- Turner, B. H., & Herkenham, M. (1991). Thalamoamygdaloid projections in the rat: A test of the amygdala's role in sensory processing. *Journal of Comparative Neurology*, 313(2), 295-325. <https://doi.org/10.1002/cne.903130208>
- Ubeda-Bañon, I., Novejarque, A., Mohedano-Moriano, A., Pro-Sistiaga, P., de la Rosa-Prieto, C., Insausti, R., ... Martinez-Marcos, A. (2007). Projections from the posterolateral olfactory amygdala to the ventral striatum: neural basis for reinforcing properties of chemical stimuli. *BMC Neuroscience*, 8, 103. <https://doi.org/10.1186/1471-2202-8-103>
- Ubeda-Bañon, I., Novejarque, A., Mohedano-Moriano, A., Pro-Sistiaga, P., Insausti, R., Martinez-Garcia, F., ... Martinez-Marcos, A. (2008). Vomeronasal inputs to the rodent ventral striatum. *Brain Research Bulletin*, 75(2-4), 467-73. <https://doi.org/10.1016/j.brainresbull.2007.10.028>
- Veening, J. G. (1978a). Cortical afferents of the amygdaloid complex in the rat: an HRP study. *Neuroscience Letters*, 8(3), 191-195. [https://doi.org/10.1016/0304-3940\(78\)90120-9](https://doi.org/10.1016/0304-3940(78)90120-9)
- Veening, J. G. (1978b). Subcortical afferents of the amygdaloid complex in the rat: an HRP study. *Neuroscience Letters*, 8(3), 197-202. [https://doi.org/10.1016/0304-3940\(78\)90121-0](https://doi.org/10.1016/0304-3940(78)90121-0)
- Vertes, R. P., Hoover, W. B., Do Valle, A. C., Sherman, A., & Rodriguez, J. J. (2006). Efferent projections of reuniens and rhomboid nuclei of the thalamus in the rat. *Journal of Comparative Neurology*, 499(5), 768-796. <https://doi.org/10.1002/cne.21135>
- Yamamoto, T., Shimura, T., Sako, N., Yasoshima, Y., & Sakai, N. (1994). Neural substrates for conditioned taste aversion in the rat. *Behavioural Brain Research* 65:123-137. [https://doi.org/10.1016/0166-4328\(94\)90097-3](https://doi.org/10.1016/0166-4328(94)90097-3)

FIGURE LEGENDS

Figure 1. Photomicrographs of cases of retrograde (A-C) and anterograde (D-F) labeling of different density. To illustrate the criteria used to rate the density of the obtained labeling, examples of very dense, moderate or very scarce labeling are shown. (A) very dense retrograde labeling in the mitral cell layer of the main olfactory bulb. (B) moderate retrograde labeling in the mitral cell layer of the accessory olfactory bulb. (C) very scarce retrograde labeling in the infralimbic cortex. Note the granular deposits of DAB in the cytoplasm (arrowhead). (D) very dense anterograde labeling in the posterolateral cortical nucleus of the amygdala, especially in its layer I. (E) moderate anterograde labeling in the ventral aspect of the CA1 of the hippocampus. (F) very scarce anterograde labeling in the medial division of the anterior olfactory nucleus (arrowhead). Scale bar in A, valid for B-F: 100 μm .

Figure 2. Photomicrographs of Nissl staining (A, B, D, E) and acetyl cholinesterase histochemistry (A', B', C', D') of transverse sections at different antero-posterior levels of the amygdaloid complex. Note the differences in acetyl cholinesterase reactivity between the cortex-amygdala transition zone and anterior cortical amygdala (A'-D') and the differences in their laminar definition (A- D). Note the loose organization of cell layers in the ACo. Scale bar in A, valid for A-C and A'- C': 500 μm . Scale bars in D and D': 500 μm

Figure 3. Injection sites of Fluorogold and BDA in the anterior cortical amygdala of mice. (A-I) Schematic drawings representing the extent of the tracer injection deposits restricted to the anterior cortical amygdaloid nucleus. The injections of Fluorogold (retrograde tracer) are represented in panels A-D; the injections of BDA (anterograde tracer) are shown in panels E-I. Single injections are identified with the animal code. (J-K) Photomicrographs through the amygdala showing representative injection sites of Fluorogold (J, fluorescence microscopy) and BDA (K). Scale bar in J, valid for K = 200 μm

Figure 4. Summary of the distribution of retrograde labeling following a Fluorogold injection in the anterior cortical amygdaloid nucleus, plotted onto schematic

drawings of parasagittal (A) and frontal (B-L) sections through the mouse brain.

The injection site is depicted in panel (C). B is rostral, L is caudal. The schematic drawings are based on the #1339, which presented the largest restricted injection site (see Fig. 3A). For abbreviations, see list.

Figure 5. Photomicrographs of parasagittal (A) and frontal (B-F) sections through the mouse brain, illustrating the retrograde labeling observed in animals receiving a Fluorogold injection in the anterior cortical amygdaloid nucleus.

The images correspond to the retrograde labeling presented in cases #1339 (A-D; injection site showed in Fig 3J) and #1245 (E, F; injection site showed in Fig. 3F-H). (A) Retrogradely labeled mitral cells in the main olfactory bulb. Inset in A shows retrograde labeling in the mitral and glomerular cell layer (see arrowheads) of the accessory olfactory bulb. (B) Retrograde labeling present in the territory between the posterior aspect of the anterior olfactory nucleus and the olfactory tubercle. (C) Numerous labeled cells in the caudal piriform cortex and dorsal part of the endopiriform nucleus within the olfactory system. In the amygdala, dense labeling is present in the posterolateral cortical amygdaloid nucleus, and a moderate labeling appears in the posteroventral and posterodorsal subdivision of the medial amygdaloid nucleus, the intraamygdaloid division of the bed nucleus of the stria terminalis and the posterior part of the basomedial amygdaloid nucleus. Note the heterogeneous distribution of the retrograde labeling in the posterodorsal Me, with the labeled cells mainly located in the external part of its cellular layer (arrowheads). At this level, the posteromedial cortical amygdaloid nucleus is almost devoid of labeling. (D) Dense retrograde labeling in the caudal part of the posteromedial cortical amygdaloid nucleus and moderate density of retrogradely labeled cells in the amygdalopiriform transition area. Within the olfactory cortex, dense labeling is present in the posterior part of the piriform cortex. (E) Numerous retrogradely labeled cells in the posterior intralaminar thalamic region. (F) Retrogradely labeled cells in the medial and lateral divisions of the parabrachial nucleus and in the locus coeruleus. For abbreviations, see list. Scale bar in A: 1 mm. Scale bar in inset in A: 250 μm . Scale bar in B (valid for B–D): 500 μm . Scale bar in E (valid for F): 200 μm .

Figure 6. Summary of the distribution of anterograde labeling following a BDA injection in the anterior cortical amygdaloid nucleus, plotted onto schematic drawings of parasagittal (A) and frontal (B-M) sections through the mouse brain. The injection

site is shown in panel (G). B is rostral, M is caudal. The schematic drawings are based on the case #1340, which presented a restricted injection site and with no BDA traces along the pipette track (photomicrograph of injection site showed in Fig. 3K). For abbreviations, see list.

Figure 7. Photomicrographs of frontal sections through the mouse brain, illustrating the anterograde labeling resulting after BDA injections in the anterior cortical amygdaloid nucleus. (A) Anterograde labeling in the dorsal peduncular cortex, the medial orbital cortex and infralimbic cortex. Inset in A shows a high magnification detail of the labeled fibers. (B) Anterograde labeling present in the basal forebrain and several structures of the central extended amygdala, such as the *substantia innominata*, the interstitial nucleus of the posterior limb of the anterior commissure and the anterior bed nucleus of the stria terminalis (BST). (C) Dense anterograde labeling next to the injection site, and in the posterior BST. Note that the labeled fibers avoid, to some extent, the nucleus of the lateral olfactory tract. Inset in C shows a high magnification detail of the labeled fibers in the different subdivisions of the posterior BST. (D) Anterograde labeling at caudal level of the amygdaloid complex. (E) Anterograde labeling in ventral hippocampus and in the ventral mesencephalon. Left inset shows a high magnification detail of the labeled fibers in the CA1. Right inset shows a high magnification detail of the labeled fibers in the *substantia nigra* and the ventral tegmental area. (F) Anterograde labeling in the brainstem, at the level of the parabrachial nucleus. Upper inset shows a high magnification detail of the labeled fibers in the lateral division of the parabrachial nucleus. Bottom inset shows a high magnification detail of labeled fibers in the *locus coeruleus*. Photomicrographs taken from case #1243. For abbreviations, see list. Scale bar in A (valid for D): 1 mm. Scale bar in B (valid for C, E, F): 1 mm. Scale bars in insets in A-E: 100 μm . Scale bars in insets in F: 50 μm .

Figure 8. Schematic representation of the pattern of afferent (A) and efferent (B) projections of the anterior cortical amygdaloid nucleus described in the present work. (C) Functional interpretation of cortical and subcortical projections to the anterior cortical amygdaloid nucleus. The thickness of the arrows roughly represents the density of the projections.

TABLE LEGENDS

Table 2. Semiquantitative rating of the density of the ipsilateral retrograde and anterograde labeling. For abbreviations, see list.

++++ very dense; +++ dense; ++ moderate; + scarce; ↓+ very scarce; 0 not found.

Accepted Article

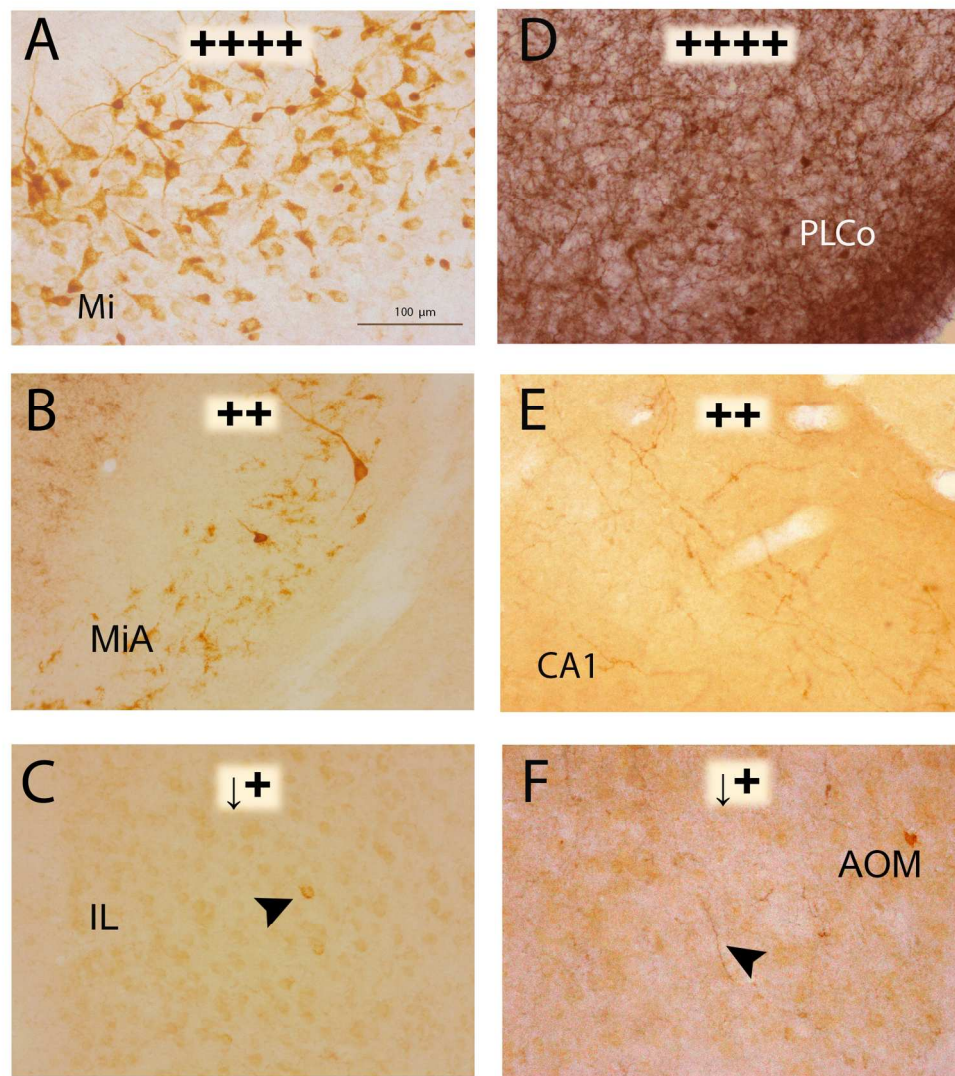


Figure 1. Photomicrographs of cases of retrograde (A-C) and anterograde (D-F) labeling of different density. To illustrate the criteria used to rate the density of the obtained labeling, examples of very dense, moderate or very scarce labeling are shown. (A) very dense retrograde labeling in the mitral cell layer of the main olfactory bulb. (B) very dense anterograde labeling in the posterolateral cortical nucleus of the amygdala, especially in its layer I. (C) moderate retrograde labeling in the mitral cell layer of the accessory olfactory bulb. (D) moderate anterograde labeling in the ventral aspect of the CA1 of the hippocampus. (E) very scarce retrograde labeling in the infralimbic cortex. Note the granular deposits of DAB in the cytoplasm (arrowhead). (F) very scarce anterograde labeling in the medial division of the anterior olfactory nucleus (arrowhead). Scale bar in A, valid for B-F: 100 μ m.

171x195mm (300 x 300 DPI)

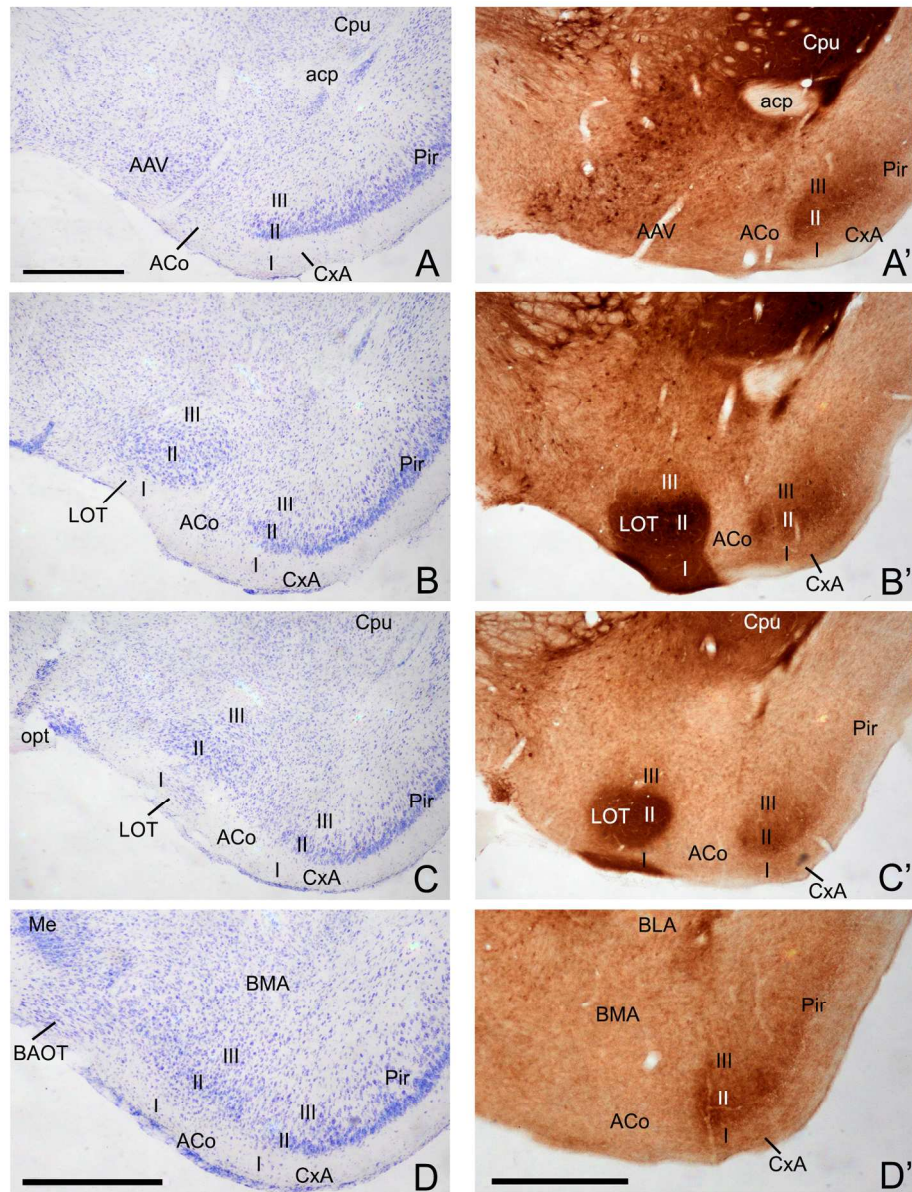


Figure 2. Photomicrographs of Nissl staining (A, B, D, E) and acetyl cholinesterase histochemistry (A', B', C', D') of transverse sections at different antero-posterior levels of the amygdaloid complex. Note the differences in acetyl cholinesterase reactivity between the cortex-amygdala transition zone and anterior cortical amygdala (A'-D') and the differences in their laminar definition (A- D). Inset in D shows the loose organization of cell layers in the ACo. Scale bar in A, valid for A-C and A'- C': 500 μ m. Scale bars in D and D': 500 μ m

171x208mm (300 x 300 DPI)

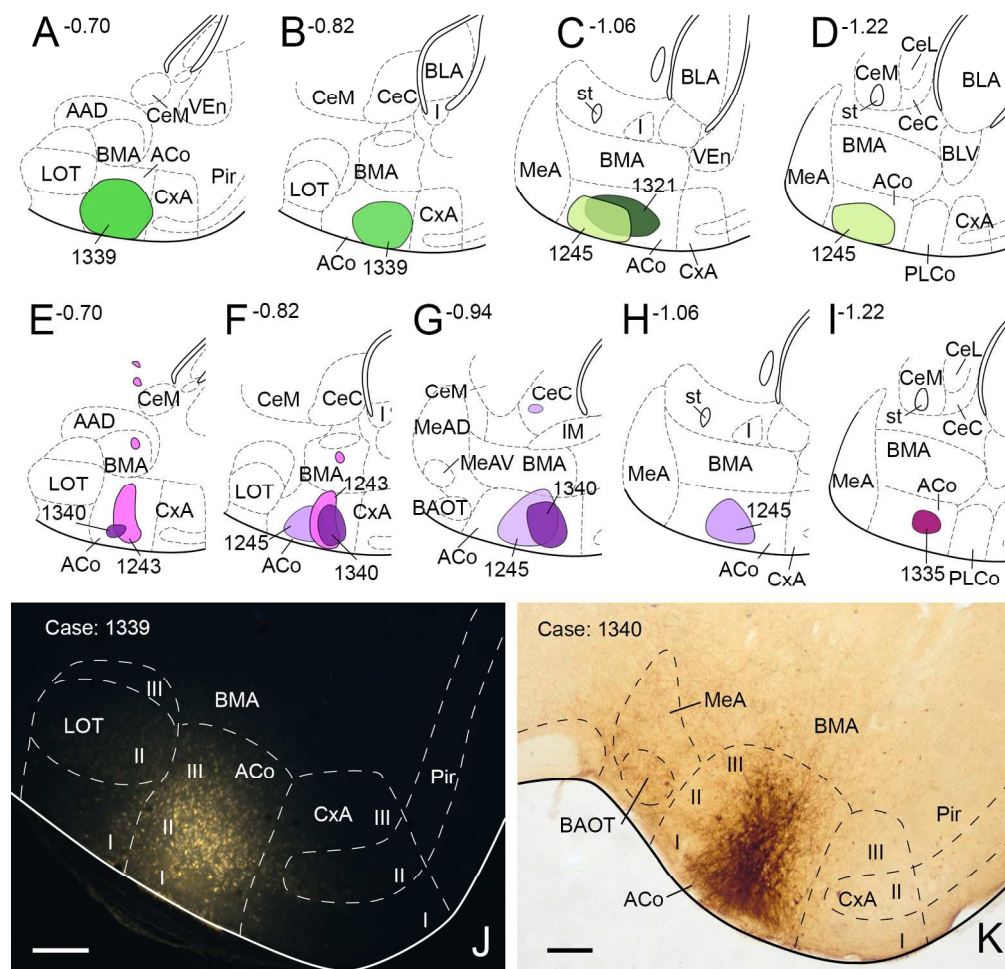


Figure 3. Injection sites of Fluorogold and BDA in the anterior cortical amygdala of mice. (A–I) Schematic drawings representing the extent of the tracer injection deposits restricted to the anterior cortical amygdaloid nucleus. The injections of Fluorogold (retrograde tracer) are represented in panels A–D; the injections of BDA (anterograde tracer) are shown in panels E–I. Single injections are identified with the animal code. (J–K) Photomicrographs through the amygdala showing representative injection sites of Fluorogold (J, fluorescence microscopy) and BDA (K). Scale bar in J, valid for K = 200 μ m

172x167mm (300 x 300 DPI)

Acc

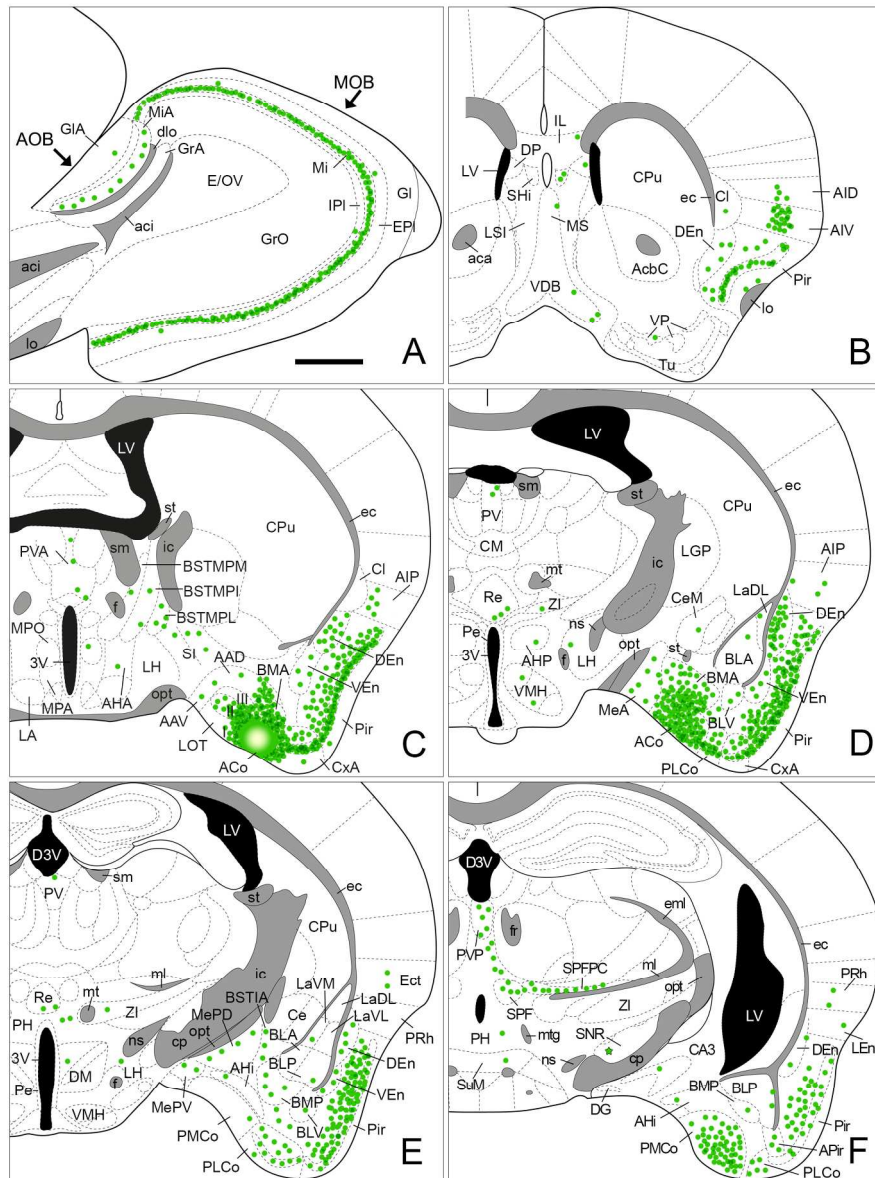


Figure 4. Summary of the distribution of retrograde labeling following a Fluorogold injection in the anterior cortical amygdaloid nucleus, plotted onto schematic drawings of parasagittal (A) and frontal (B-L) sections through the mouse brain. The injection site is depicted in panel (C). B is rostral, L is caudal. The schematic drawings are based on the #1339, which presented the largest restricted injection site (see Fig. 3A). For abbreviations, see list.

176x235mm (300 x 300 DPI)

A

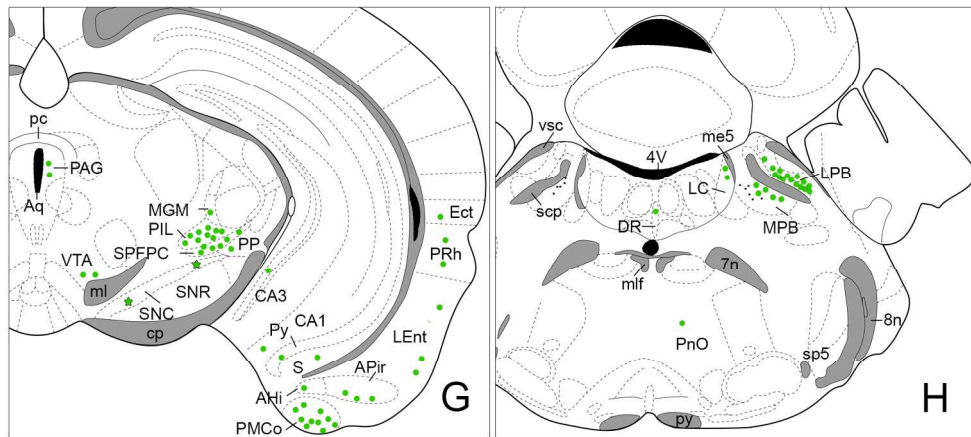


Figure 4 (continuation)

176x81mm (300 x 300 DPI)

Accepted

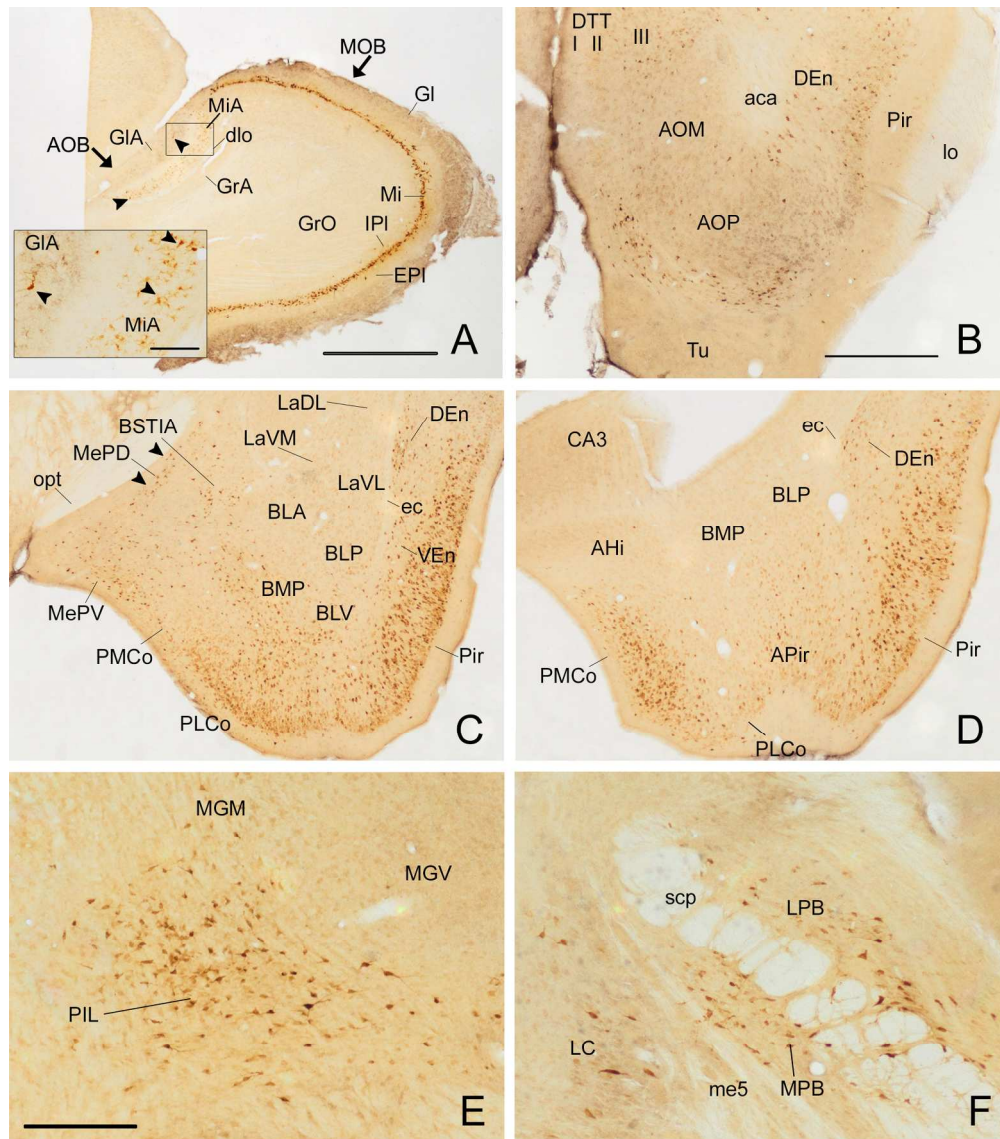


Figure 5. Photomicrographs of parasagittal (A) and frontal (B-F) sections through the mouse brain, illustrating the retrograde labeling observed in animals receiving a Fluorogold injection in the anterior cortical amygdaloid nucleus. The images correspond to the retrograde labeling presented in cases #1339 (A-D; injection site showed in Fig 3J) and #1245 (E, F; injection site showed in Fig. 3F-H). (A) Retrogradely labeled mitral cells in the main olfactory bulb. Inset in A shows retrograde labeling in the mitral and glomerular cell layer (see arrowheads) of the accessory olfactory bulb. (B) Retrograde labeling present in the territory between the posterior aspect of the anterior olfactory nucleus and the olfactory tubercle. (C) Numerous labeled cells in the caudal piriform cortex and dorsal part of the endopiriform nucleus within the olfactory system. In the amygdala, dense labeling is present in the posterolateral cortical amygdaloid nucleus, and a moderate labeling appears in the posteroventral and posterodorsal subdivision of the medial amygdaloid nucleus, the intraamygdaloid division of the bed nucleus of the stria terminalis and the posterior part of the basomedial amygdaloid nucleus. Note the heterogeneous distribution of the retrograde labeling in the posterodorsal Me, with the labeled cells mainly located in the external part of its cellular layer (arrowheads). At this level, the posteromedial cortical amygdaloid nucleus is almost devoid of labeling. (D) Dense retrograde labeling in the caudal part of the posteromedial cortical amygdaloid nucleus and moderate

density of retrogradely labeled cells in the amygdalopiriform transition area. Within the olfactory cortex, dense labeling is present in the posterior part of the piriform cortex. (E) Numerous retrogradely labeled cells in the posterior intralaminar thalamic region. (F) Retrogradely labeled cells in the medial and lateral divisions of the parabrachial nucleus and in the locus coeruleus. For abbreviations, see list. Scale bar in A: 1 mm. Scale bar in inset in A: 250 μm . Scale bar in B (valid for B–D): 500 μm . Scale bar in E (valid for F): 200 μm .

171x195mm (300 x 300 DPI)

Accepted Article

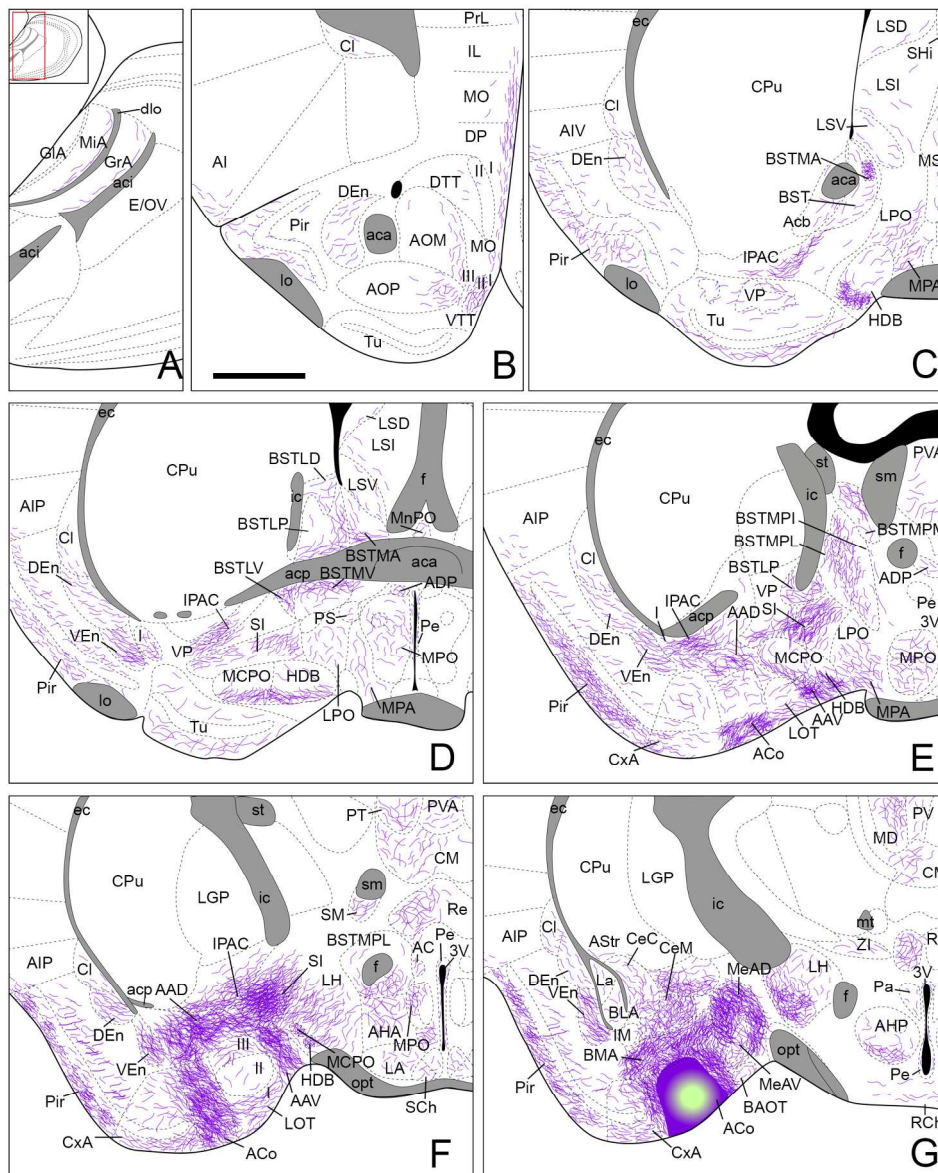


Figure 6. Summary of the distribution of anterograde labeling following a BDA injection in the anterior cortical amygdaloid nucleus, plotted onto schematic drawings of parasagittal (A) and frontal (B-M) sections through the mouse brain. The injection site is shown in panel (G). B is rostral, M is caudal. The schematic drawings are based on the case #1340, which presented a restricted injection site and with no BDA traces along the pipette track (photomicrograph of injection site showed in Fig. 3K). For abbreviations, see list.

172x218mm (300 x 300 DPI)



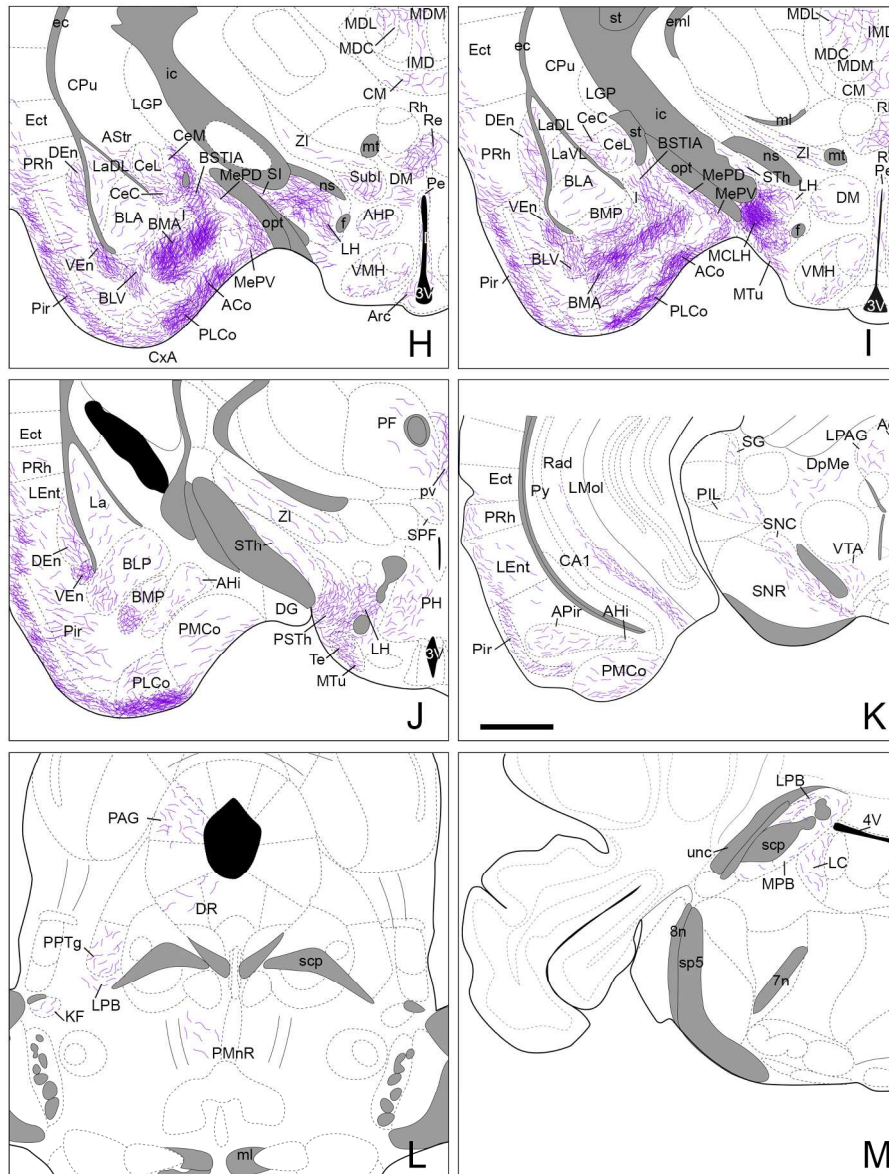


Fig. 6 (continuation)

172x230mm (300 x 300 DPI)

AC

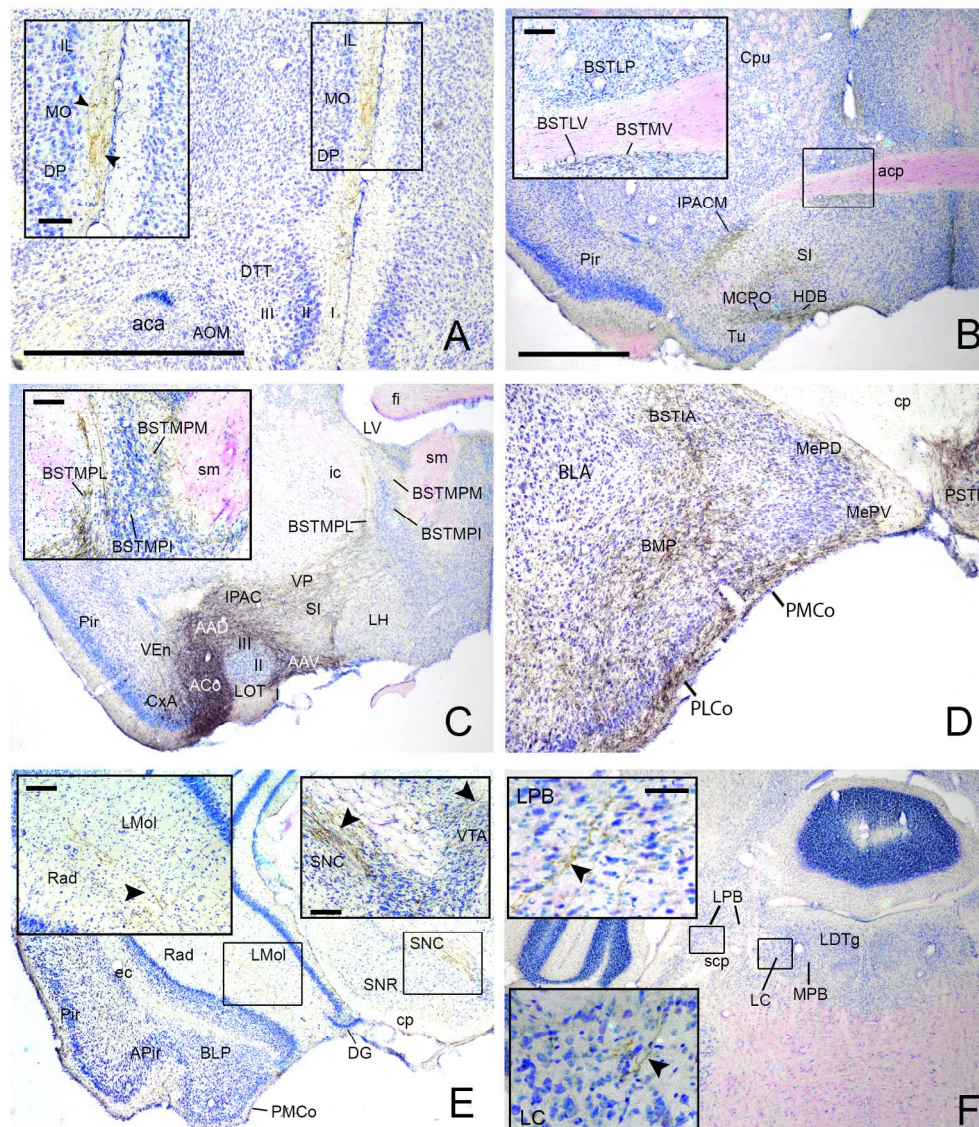


Figure 7. Photomicrographs of frontal sections through the mouse brain, illustrating the anterograde labeling resulting after BDA injections in the anterior cortical amygdaloid nucleus. (A) Anterograde labeling in the dorsal peduncular cortex, the medial orbital cortex and infralimbic cortex. Inset in A shows a high magnification detail of the labeled fibers. (B) Anterograde labeling present in the basal forebrain and several structures of the central extended amygdala, such as the substantia innominata, the interstitial nucleus of the posterior limb of the anterior commissure and the anterior bed nucleus of the stria terminalis (BST). (C) Dense anterograde labeling next to the injection site, and in the posterior BST. Note that the labeled fibers avoid, to some extent, the nucleus of the lateral olfactory tract. Inset in C shows a high magnification detail of the labeled fibers in the different subdivisions of the posterior BST. (D) Anterograde labeling at caudal level of the amygdaloid complex. (E) Anterograde labeling in ventral hippocampus and in the ventral mesencephalon. Left inset shows a high magnification detail of the labeled fibers in the CA1. Right inset shows a high magnification detail of the labeled fibers in the substantia nigra and the ventral tegmental area. (F) Anterograde labeling in the brainstem, at the level of the parabrachial nucleus. Upper inset shows a high magnification detail of the labeled fibers in the lateral division of the parabrachial nucleus. Bottom inset shows a high magnification detail of labeled fibers in the locus coeruleus. Photomicrographs taken from

case #1243. For abbreviations, see list. Scale bar in A (valid for D): 1 mm. Scale bar in B (valid for C, E, F): 1 mm. Scale bars in insets in A-E: 100 μ m. Scale bars in insets in F: 50 μ m.

171x195mm (300 x 300 DPI)

Accepted Article

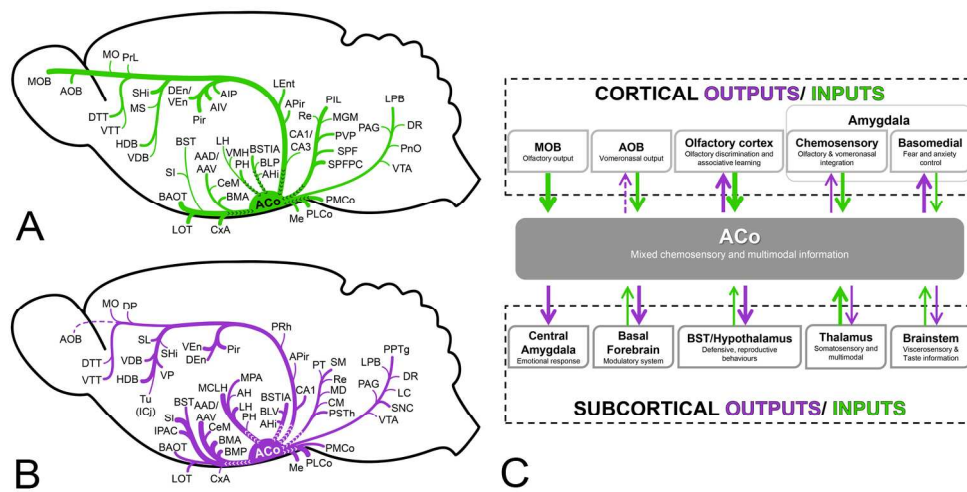


Figure 8. Schematic representation of the pattern of afferent (A) and efferent (B) projections of the anterior cortical amygdaloid nucleus described in the present work. (C) Functional interpretation of cortical and subcortical projections to the anterior cortical amygdaloid nucleus. The thickness of the arrows roughly represents the density of the projections.

176x93mm (300 x 300 DPI)

Accepte

Table 1. Anti-fluorogold primary antibody information

Antigen	Immunogen	Manufacturer, Host species, Ig isotype, Catalog number and RRIDs	Dilution used in IHC
Fluorogold	Fluorogold (5-hydroxystabilamide)	Merck-Millipore, Temecula, CA. Rabbit, polyclonal, AB-153, RRID: AB_90738	1:3,000

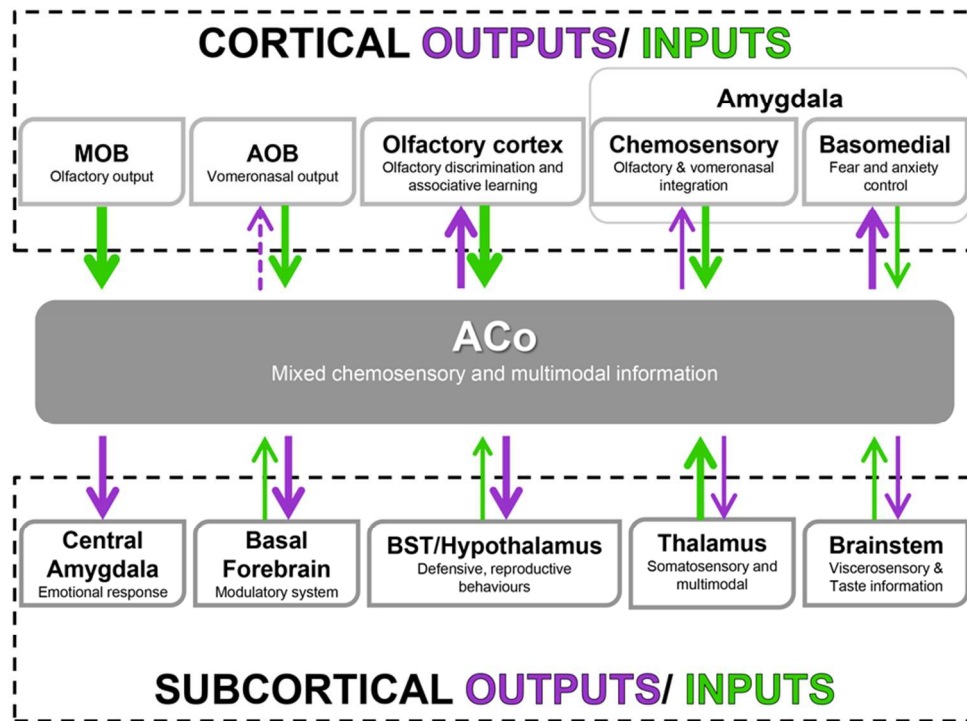
Table 2. Distribution of the ipsilateral retrograde and anterograde labeling obtained after tracer injections in the anterior cortical amygdaloid nucleus.

		FG ACo (retrograde)	BDA ACo (anterograde)
OLFACTORY SYSTEMS			
Accessory Olfactory Bulb	MiA	++	↓+
	GrA	0	↓+
Main Olfactory Bulb	Mi	++++	0
Olfactory Cortex	DTT/VTT	++/+	+ / ++
	AOL	+	↓+
	AOM	↓+	↓+
	AOV	0	↓+
	AOP	+	+
	rostral Pir	++	++
	caudal Pir	+++	+++
	DEn/VEn	+++ / +++	++ / +++
AMYGDALA and BST			
Vomeronasal amygdala	AAV/AAD	++ / ++	++++ / +++++
	BAOT	++++	++
	MeA	++	++++
	MeAV/MeAD	++ / ++	+++ / +++++
	MePV	++	+++
	MePD	++	+++
	PMCo	+++	++
Olfactory amygdala	ACo	INJECTION	INJECTION
	CxA	+++	++
	LOT	+++	++
	PLCo	+++	++++
	APir	++	+
Amygdalohippocampal transition area	AHi	+	+
Basolateral complex	BLA	↓+	+
	BLP	+	+
	BLV	+	++
	BMA	++	++++
	BMP	++	+++
	LaDL	+	+
	Central	CeL	↓+
CeM		+	++
CeC		0	+
Astr		0	↓+
I		↓+	+
BST	BSTIA	++	+++
	BSTMA	↓+	+
	BSTMV	↓+	++

	BSTMPM	+	++
	BSTMPI	++	++
	BSTMPL	+	+
	BSTLD	0	+
	BSTLV	↓+	++
	BSTLP	↓+	+
CORTEX AND HIPPOCAMPAL FORMATION			
Cortex	AID/AIV	+ / +++	0 / ↓+
	AIP	++	↓+
	PrL	+	↓+
	IL	↓+	+
	DP	↓+	+
	MO	+	+
	Cg	0	↓+
	Cl	↓+	↓+
	PRh	+	+
	Ect	+	↓+
Hippocampal formation	CA1	+	++
	CA3	+	0
	S	+	0
	LEnt	++	+
SEPTUM / BASAL FOREBRAIN			
Lateral septal complex	LSD	0	↓+
	LSI	↓+	↓+
	LSV	0	↓+
	SHy	0	↓+
	SHi	+++	+
Medial septum/ Diagonal band	HDB/MCPO	++	+++
	VDB	+	++
	MS	+	↓+
Striato-pallidum	AcbC/AcbSh	0	+ / ↓+
	ICj	0	+
	Tu	0	+
	VP	+	++
	IPAC	↓+	+++
	SI	+	++++
	SL	↓+	++
PREOPTIC REGION			
Preoptic	MPA	↓+	++
	MPO	↓+	++
	LPO	0	+
	AC	0	+
	ADP	0	+
	PS	0	↓+

HYPOTHALAMUS			
Anterior	AH	↓+	↓+
	LA	0	↓+
Tuberal	Pa	0	↓+
	Pe	0	↓+
	SCh	0	↓+
	RCh	0	↓+
	DM	0	↓+
	LH	+	+++
	MCLH	0	++++
	VMH	+	+
	PH	++	+
	MTu	0	++
	Te	0	++
	TC	↓+	+
Mamillary	Arc	0	↓+
	STh	0	↓+
	PSTh	0	+
	PMD/PMV	↓+/↓+	↓+/+
	SuM	↓+	+
THALAMIC COMPLEX			
Prethalamus	ZI	↓+	↓+
	Subl	0	+
Thalamus	LHb	0	↓+
	PVA/PV	+/↓+	↓+
	PVP	++	↓+
	pv	++	+
	PT	0	+
	CM	0	+
	SM	0	++
	IMD	0	↓+
	MD	0	+
	Re	+	+
	PF	0	↓+
	SPF	++	↓+
	SPFPC	+++	↓+
	SG	↓+	↓+
	MGM	+	0
PIL	+++	↓+	
POT	0	↓+	
PP	+	↓+	
MIDBRAIN and BRAINSTEM			
	PAG	+	+
	VTA	+	+

	DpMe	0	↓+
	RPC	0	↓+
	SNC	0	+
	SNR	0	+
	DR	+	↓+
	PMnR	0	↓+
	PnO	↓+	0
	PPTg	0	++
	LPB	++	+
	MPB	+	↓+
	KF	0	↓+
	LC	+	+
	RLi	↓+	0



86x64mm (300 x 300 DPI)

Accept

Summary and functional interpretation of cortical and subcortical projections to the anterior cortical nucleus of the amygdala.

Accepted Article